Responses to Anonymous Referee #1

Thank you for your positive review of our manuscript. We sincerely appreciate the efforts you have put in the review process, and we improve this work based on your comments and suggestions. Below we will respond to your comments one by one. Your comments are in bold italics, and my responses are in plain text. All the changes have been included in the newest version of our manuscript.

Major comments:

1. ***One major comment arises from the lacking descriptions about the measurement techniques, H-TDMA. I could not get any information about the experimental protocols and technical details about the study methods, such as the configuration of HTDMA used in this study, how aerosols were generated and dried, how aerosols get charged (soft X-ray ionization or corona discharge)c, the number concentration of aerosols, etc. Elaborating these points would put this study in better context.***
   Response: Thank you for your comment. Based on your suggestion and concern, more information on this part has been added in our new manuscript in section 4.

2. ***Page 1, line 21-26: This paragraph needs improvements. The authors tried to describe the significance of aerosol's hygroscopicity to state their motivations to study the effects of multi-charge on aerosols. However, the current version was too short and brief to state the environmental, climate as well as the health effects of atmospheric aerosols. Furthermore, citing more classical and recent references.***
   Response: The introduction has been updated to include more information about the climatic and environmental effects of atmospheric aerosols, especially specifying the role of hygroscopic properties. The following is cited from the new introduction:
   'Atmospheric particles can scatter solar radiation and absorb longwave radiation, imposing direct effects on the Earth's radiation balance (Haywood and Boucher, 2000;Bond et al., 2013). They can also indirectly affect the climate through acting as cloud nuclei and modify the cloud optical properties and life cycle (ALBRECHT, 1989;Twomey, 1974;CHARLSON et al., 1992). Both these two effects are closely related to aerosol particle's hygroscopicity, which describes the particle's ability to absorb water at sub or supersaturated conditions (e.g. McFiggans et al., 2006). Aerosol hygroscopicity also plays a vital role in environmental aspects. It has been reported to be an important factor regulating environmental visibility because it can greatly enhance the particle's

light scattering efficiency and degrade visibility under relatively high relative humidity (Chen et al., 2012;Xu et al., 2020). It can increase aerosol particle's liquid water content, affect the multiphase chemistry and local photochemistry, and facilitates particle formation and aging processes (Wu et al., 2018;Herrmann et al., 2015;Ervens et al., 2011). For human health, aerosol hygroscopicity directly determines the particle's size, thus modifying the deposition pattern of inhaled particles in the human respiratory tract (Heyder et al., 1986;Löndahl et al., 2007). In general, aerosol particle's hygroscopicity is one of the most important properties when quantifying the particle's climatic and environmental effects. It's also useful to characterize the particle's detailed chemical information. Therefore, it's necessary to offer a correct and detailed measurement of aerosol hygroscopicity.'

3. ***Section 3.2: For ambient aerosols, there are different mixing states, e.g., internal, external and core-shell structures, whether this factor has an impact on the multi-charge correction results and has been considered in the algorithm?***
   Response: The mixing state doesn't impact our multi-charge correction results because the charge distribution and DMA sizing process is only related to the particle size (Wiedensohler et al., 1986), not affected by the mixing state. In the algorithm, only the measured mean hygroscopicity is used in the correction.

Minor comments:

1. ***Authors should fix the typo and format mistakes of references through the whole manuscript, especially in the References section.***
   Response: Thank you for your comment. We double checked our manuscript and corrected the typos and format mistakes.

2. ***Page 1, line 28: I notice that aerosol hygroscopicity measurement techniques have been reviewed in a recent study (Tang et al., 2019, ACP), please cite it.***
   Response: This citation has been added to our new manuscript.

3. ***Page 1, line 29, 30: Swietlicki et al., 2017 should be Swietlicki et al., 2008.***
   Response: We updated this citation in the new manuscript.

4. ***Page 4, line 100: The results are summarized in Fig. 3b and Table 1.***
   Response: Thank you for your comment. It has been added in the text.

5. ***Page 6, line 171: Please give some information about the sampling site.***
   Response: We added some site descriptions in the section 4.

6. ***Page 7, line 195: How large? I suggest that authors provide more discussions based on their field measurement results.***
   Response: We have another academic paper focusing on the measurement results (Shen et al., 2020). We added this citation in the manuscript for reference.

Responses to Anonymous Referee #2

General comments:

Shen et al. present a new algorithm for the size-resolved correction of the hygroscopicity, κ considering shrinking effect caused by to multi-charge number contribution. I recommend this manuscript to be published in AMT after the following issues to be addressed and modified.

General response: Thank you very much for your review of our manuscript. Your comments were very helpful and constructive in improving this work. Below we will respond to your comments one by one. Your comments are in bold italics, and my responses are in plain text. In the end of this reply, we also attach our supplement materials.

Major comments:

1. ***The term "shrinking effect" seems to be unfortunate, since it used for actual irregular particles restructuring in the humid conditions caused by surface or capillary forces of absorbed/adsorbed water. To avoid confusion, I recommend using another term, say "compression effect" or "displacement effect".***
   Response: In the AMTD preprint version, we use the term 'weakening effect'. But after your comment, we think the term 'compression effect' is better and this term is being used now in the new manuscript. Thank you for your suggestion!

2. ***The shrinking function S (ι, ν) is not properly described in the text. Please show which expression/algorithm was used to calculate it.***
   Response: Thank you for your suggestion. I added an algorithm flowchart in the manuscript.
   The calculation mainly involves four steps: (1) calculate the f function as illustrated in supplement section 2, and the f function is used to calculate the physical diameter of multiply charged particles; (2) for each combination of (D_p^* , ν), generate different g_0 data points and obtain the corresponding g_{DMA} from the equation 10. Then transform the GF space (g_0, g_{DMA}) to the hygroscopicity space (κ, κ_{DMA}) according to the κ-kohler theory; (3) Fit the (κ, κ_{DMA}) with a straight line across the origin and obtain the slope as the compression factor; (4) repeat the step 2-3 for different combination of (D_p^* , ν). The figure below is the algorithm procedures.

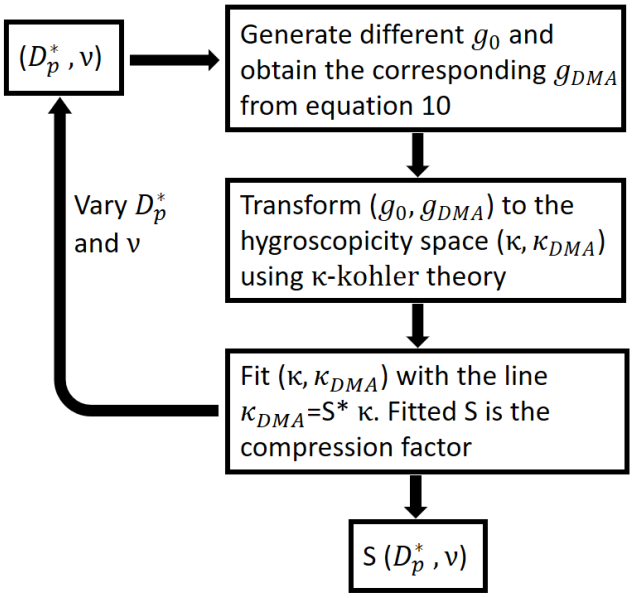

3. ***The multi-charge algorithm for hygroscopicity correction has not been properly tested. As a first step, I would suggest to apply it for single-component particles (100; 200, and 300 nm) with well-defined thermodynamic and hygroscopic properties, ammonium sulfate as an example. Please show the particle's growth factors change taking into account F(x,v), Ω(x,v,i) and S(i, v) and then κ initial and κ corrected as a function RH.***

Response: Thank you for your suggestion. The following is a test for our correction algorithm.
In general, the algorithm cannot ensure that the corrected particle's size-resolved hygroscopicity is fully consistent with the true values because of the measurement size resolution (detailed hygroscopicity information between measured size is lost), but the correction can bring the results closer to the true values.

If we assume a group of ammonium sulfate particles with a constant κ of 0.53. Then the HTDMA is used to scan these aerosol particles. The sample/sheath ratio of the first DMA is 1/10 and the DMA will select those negatively charged particles (DMA type from BMI). According to the following two equations:

$$\mathrm{N}\left(D_p^*\right) = \int_0^\infty G\left(D_p^*, x\right) n(x) dx$$

$$\mathrm{G}\left(D_p^*, x\right) = \sum_{v=1}^{\infty} F(x, v)\Omega\left(x, v, D_p^*\right)$$

the kernel function for each size set in DMA is shown below with the assumed particle number size distribution.

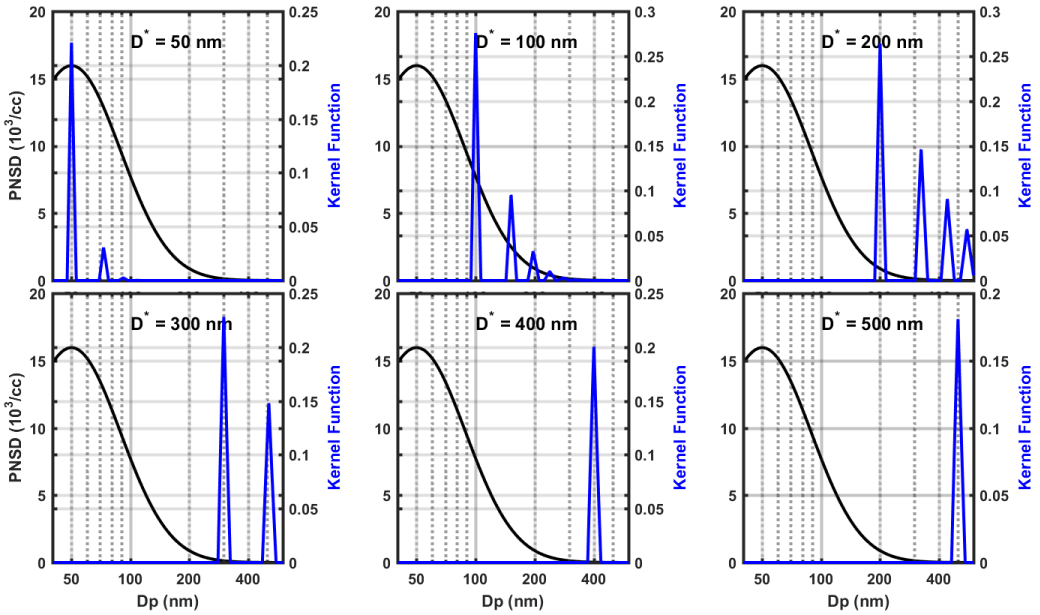

Fig.1: The black lines are the assumed ammonium sulfate particle's number size distribution. The blue lines are the kernel functions for the diameter set labelled in the panel.

Then we use the HTDMA to obtain the size-resolved hygroscopicity over the size of [50,100,150, 200,250, 300,400,500,600] (nm). For each diameter set D_p^* in the first DMA, it will give the corresponding measured hygroscopicity as the following equations:

$$K^*(D_p^*) = \frac{1}{N(D_p^*)} \int_0^\infty G_s(D_p^*, x)\mathrm{K}(x)n(x)dx$$

$$G_s(D_p^*, x) = \sum_{v=1}^{\infty} F(x, v)\Omega(x, v, D_p^*)S(D_p^*, v)$$

Based on our calculation, we can obtain the $K^*(D_p^*)$. Then we apply our multi-charge correction algorithm in the calculated $K^*(D_p^*)$ and retrieve a corrected one. The results are listed in the figure below.

The black line is the true hygroscopicity distribution with a uniform κ of 0.53. It can be seen that the measured $K^*(D_p^*)$ deviate much from the true distributions because of multi-charge effect. The sizes of 100 and 150 nm are influenced most because the high ratio of multiply charged particles. After the correction, the hygroscopicity distribution comes very close to the true value. The large error at the size of 50 nm is due to the missing information between 50 nm and 100 nm, and the size of 50 nm is mostly affected by particles from this size range. If the measurement size resolution improves, the corrected values will come closer to the true values.

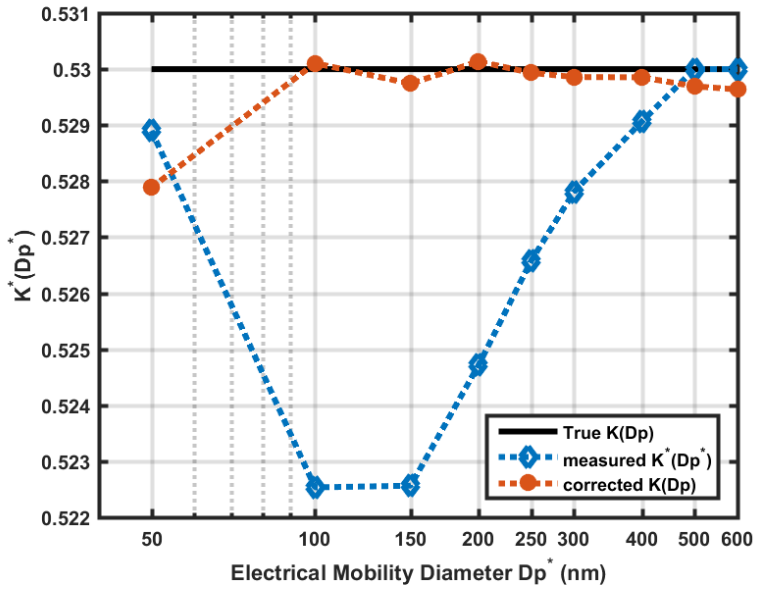

4. ***Due to typos and errors, the text is difficult to read.***
   Response: Thank you for your detailed review of this manuscript. We double checked the paper and fixed all the errors.

Minor comments:

1. ***Page 1, line 30: Swietlicki et al. should be Swietlicki et al., 2008;***
   Response: We corrected this citation in the new manuscript.

2. ***Page 2, Line 33: (Cubison, Coe, & Gysel, 2005; Gysel, McFiggans, & Coe, 2009; Stolzenburg & McMurry, 2008; Voutilainen, Stratmann, & Kaipio, 2000). Correct citation according to AMT instruction.***
   Response: We corrected this citation.

3. ***Line 41: "Duplissy et al. (2008) obtained …" Note, Gysel et al., 2009 obtained the kernel function, Duplissy et al. (2008) just used it for multi-charge correction.***
   Response: Thank you, and we have revised this part.

4. ***Line 42 "GFs" The abbreviation is not defined.***
   Response: We added the definition of GFs in the text.

5. ***Page 3, Line 70, please define the scale parameter x once.***
   Response: We removed other unnecessary definition.

6. ***Line 74, term n(x) is not defined.***
   Response: Definition added to the manuscript.

7. ***Line 77, Fig, 1b. The corresponding ratio of particles carrying different charges is calculated from the PNSD using the abovementioned DMA electrical mobility and charging theory. Please specify in detail how data in Fig.1b were obtained? Show in the explicit form the $F(x,v)$ and $\Omega(x,v,i)$, at least in Supplement.***
   Response: We added the detailed calculation procedures in the supplement section 1. In the text, we take DMA set size of 100 nm as an example and show that how we come to the final ratio of particles carrying different charges.

8. ***Line 80 For example, when we set 100 nm in the first DMA, more than 40% of the selected particles are multiply charged. Please double check a 40 % value. How it was obtained?***
   Response: As the response to the comment 7, the detailed calculation procedure is shown in the supplement. The value of 40% is reliable.

9. ***Page 3, line 88. An illustration figure (Fig.2) was shown to explain the cause of this shrinking effect Correct the sentence.***
   Response: Change made.

10. ***Page 4, Line 117 …where x is the scale parameter. It was defined in page 3, line 70.***
    Response: This definition has been deleted in the section 3.

11. ***Line 122 So the question can be simplified as the following. Change to equation.***
    Response: Change made.

12. ***Page 5, Line 132 One hypothetical κ distribution along with the corresponding multi-charge corrected κ distributions are shown in Fig.4. Here is discrepancy between "hypothetical κ distribution" in the text and "measured κ distribution" in the Fig.4 captions. Is it measured or hypothetical κ distribution?***
    Response: The κ distribution is hypothetical uncorrected values. We assume an uncorrected measurement result, and then we applied our correction algorithm to this distribution to find out the true κ distribution.

13. ***Page 6, Line 156, Eq.(12) $C(i,x)$ represents the correction factor caused by the shrinking effect In Eq.(6) the correction factor was defined as $S(i, v)$. Is it the same or new one?***

Response: It is a new one. Correction factors for different parameters (here is hygroscopicity and LH fraction) are not the same.

14. ***Line 160, … the question can be simplified into… Change to equation.***
    Response: Change made.

15. ***Line 167 … distributions are also shown in Fig.4. Change to Fig.5.***
    Response: Change made.

16. *References Page 9, line 283*
    Wiedensohler, A., Lütkemeier, E., Feldpausch, M., & Helsper, C. (1986). Investigation of the bipolar charge distribution at various gas conditions. Journal of Aerosol ence, 17(3), 413-416.
    Should be:
    Wiedensohler, A., Lütkemeier, E., Feldpausch, M., and Helsper, C.: Investigation of the bipolar charge distribution at various gas conditions, J. Aerosol Sci., 17, 413-416, https://doi.org/10.1016/0021-8502(86)90118-7, 1986.
    Please follow the AMT instruction for paper submission, especially references and citation section.
    Response: We fixed all the reference and citation format mistakes in the new manuscript.

Supplement for

Effects of Multi-Charge on Aerosol Hygroscopicity Measurement by HTDMA

Chuanyang Shen[1], Gang Zhao[1,2], Chunsheng Zhao[1]

[1]Department of Atmospheric and Oceanic Sciences, School of Physics, Peking University, Beijing 100871, China
[2]College of Environmental Sciences and Engineering, Peking University, Beijing 100871, China

1. The procedures of calculating the number ratio of particles carrying different charges.

Step 1. Calculate the particle charge distribution.

The particle charge distribution at each size is based on a theoretical model developed by Wiedensohler et al. (1986). To calculate the fraction of particles carrying zero, one or two charges, use the equation below:

$$f(D_p, N) = 10^{\left[\sum_{i=0}^{5} a_i(N)(log\frac{D_p}{nm})^i\right]}$$

$a_i(N)$	N=-2	N=-1	N=0	N=1	N=2
a_0	-26.3328	-2.3197	-0.0003	-2.3484	-44.4756
a_1	35.9044	0.6175	-0.1014	0.6044	79.3772
a_2	-21.4608	0.6201	0.3073	0.4800	-62.8900
a_3	7.0867	-0.1105	-0.3372	0.0013	26.4492
a_4	-1.3088	-0.1260	0.1023	-0.1553	-5.7480
a_5	0.1051	0.0297	-0.0105	0.0320	0.5049

For the fraction of particles carrying three or more charges, use the equation below:

$$f(D_p, N) = \frac{e}{\sqrt{4\pi^2\varepsilon_0 D_p \kappa T}} \exp \frac{-\left[N - \frac{2\pi\varepsilon_0 D_p \kappa T}{e^2}\ln(\frac{Z_{i+}}{Z_{i-}})\right]^2}{2\frac{2\pi\varepsilon_0 D_p \kappa T}{e^2}}$$

where e is the elementary charge of 1.60217733E-19 coulomb; ε_0 is the dielectric constant of 8.854187817E-12 farad/m; the D_p is the particle diameter in [m]; κ is the Boltzmann's constant of 1.380658E-23 joule/K; T is the temperature in [K]; N is the number of elementary charge units; $\frac{Z_{i+}}{Z_{i-}}$ is the ion mobility ratio of 0.875.

Here we present bipolar particle charge distribution with number of charges up to 4 over the size range of 10-1000 nm.

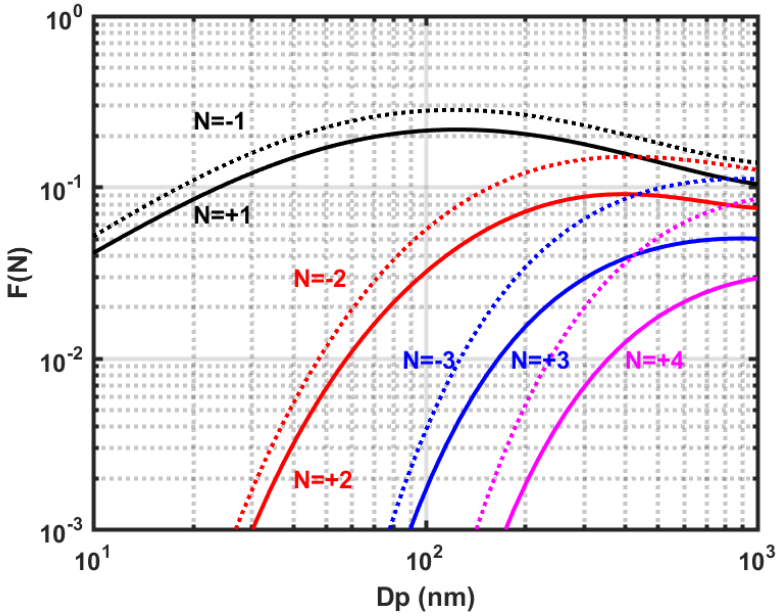

Fig.S1: Calculated number fraction of bipolar charged particles as a function of particle size. Curves decreasing in maximum charged fraction from left to right represent particles with 1 through 4 charges respectively.

Step 2: Calculate the DMA transfer function and Kernel function for each size set at DMA. In our field measurement, the DMA (BMI, Model 2100) selected those negatively charged particles. The sample/sheath ratio of 0.75/4 is used to calculate the transfer function. Then the Kernel function can be obtained from:

$$\mathrm{G}\left(D_p^*, x\right) = \sum_{v=1}^{\infty} F(x, N)\Omega(x, N, D_p^*)$$

The following is an example for the DMA set size of 100 nm.

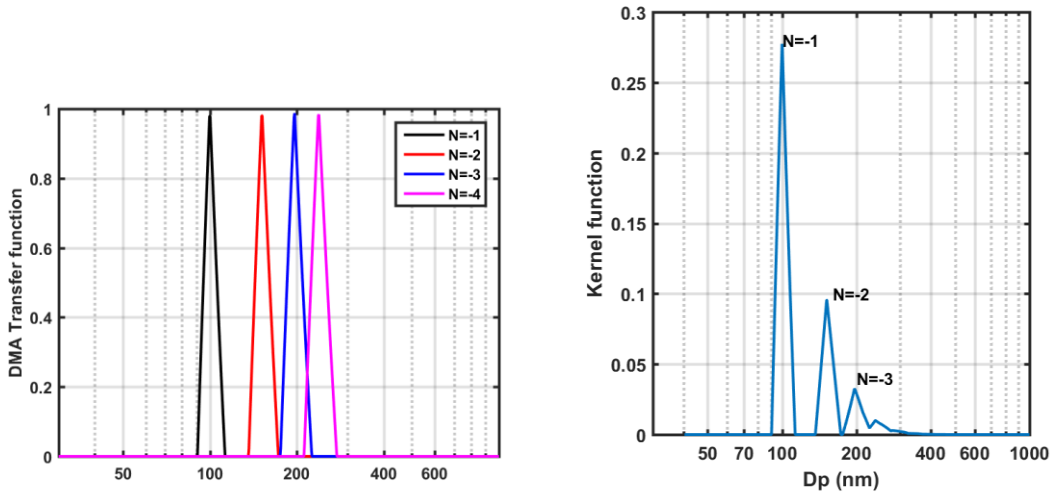

Fig.S2: The left figure is the calculated DMA transfer function for the DMA set size of 100 nm for different charges carried. The right figure is the calculated Kernel function of particles as a function of particle size. Triangle peaks from left to right represent particles with increasing number of charges.

Step 3. Calculate the (1) the total number concentration of particles that can pass through the DMA and (2) the number concentration of particles carrying v charges. In this step, particle number size distribution data is needed.

$$\mathrm{N}(D_p^*) = \int_0^\infty G\left(D_p^*, x\right) n(x) dx$$

$$N_v(D_p^*) = \int_0^\infty G_v\left(D_p^*, x\right) n(x) dx$$

Here we present a particle number size distribution data during the relatively polluted period in our field measurement. When combined with the total kernel function or charge-resolved kernel function, we can obtain the corresponding number concentration of particles that can pass through the DMA. Fig.S3 shows an example when the DMA set size is 100 nm. It can be seen that when the accumulation mode particles increase, the doubly or triply charged particles also increase greatly. In this case, when integrated over the whole size range, the singly charged particles only constitute 55% of all the particles that can pass through the DMA.

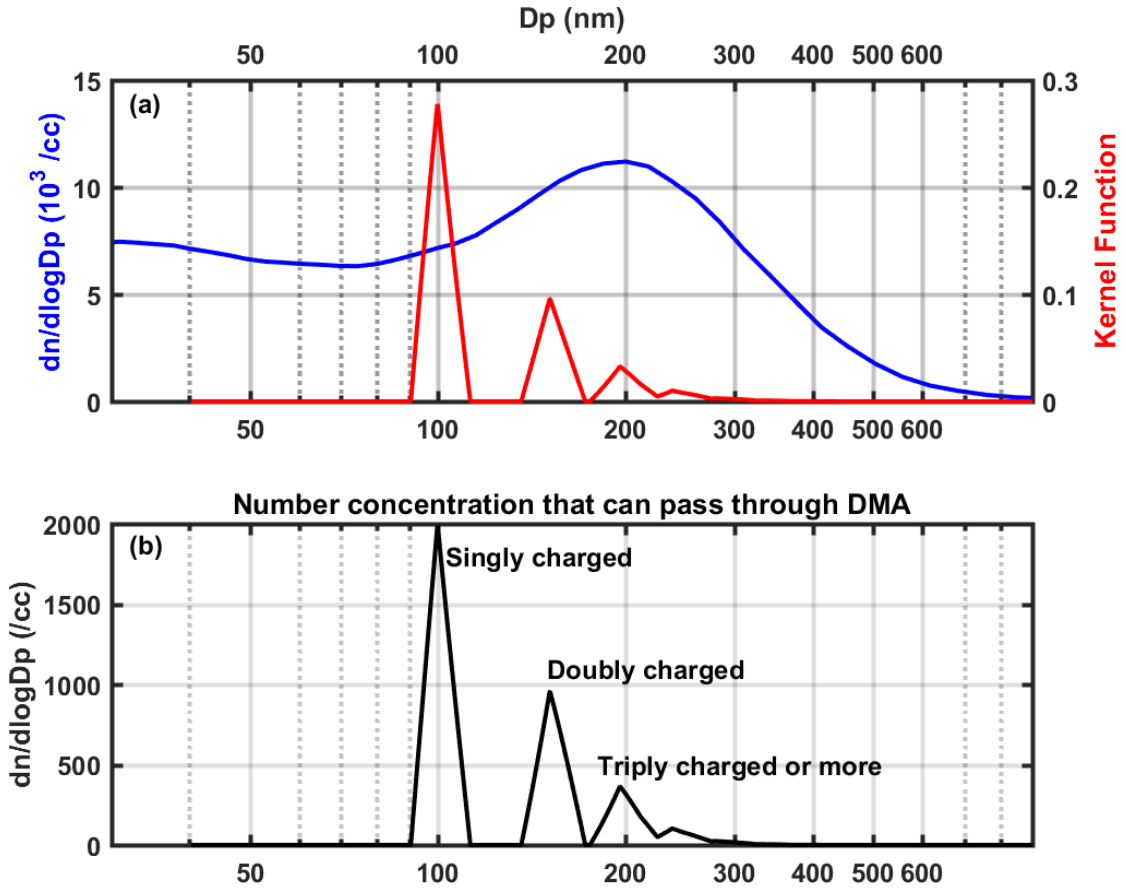

Fig.S3: (a) The blue line represents the measured particle number size distribution. The red line represents the calculated kernel function for DMA set size of 100 nm. (b) Calculated number concentration of particles that can pass through the DMA when the DMA set diameter is 100 nm. Triangle peaks from left to right represent particles with increasing number of charges.

2. The calculation and properties of f function

In the paper, f function is defined as:

$$D_p^{\nu} = f\left(D_p^*, \nu\right)$$

It describes the physical diameter of charged particles with the known parameters of electrical mobility diameter (D_p^*) and number of charges (ν).

We don't have an analytical expression for f function, but it can be calculated through two steps:

(1) Calculate the electrical mobility Z_p from D_p^* using the following equation:

$$Z_p = \frac{eC(D_p^*)}{3\pi\mu D_p^*}$$

(2) Solve the following nonlinear equation and get the best fit D_p^ν through the optimization method.

$$Z_p = \frac{\nu e\, C(D_p^\nu)}{3\pi\mu\, D_p^\nu} = \frac{eC(D_p^*)}{3\pi\mu D_p^*}$$

It will simplify into:

$$\frac{\nu\, C(D_p^\nu)}{D_p^\nu} = \frac{C(D_p^*)}{D_p^*}$$

The Cunningham slip correction C can be calculated as:

$$\mathrm{C} = 1 + \mathrm{Kn}[\alpha + \beta \exp(\frac{-\gamma}{Kn})]$$

where $\alpha = 1.142$, β=0.558, γ=0.999 (Allen & Raabe, 1985). Kn is the Knudsen Number of $2\lambda/D_p$, and λ is the gas mean free path with the expression of $\lambda_r(\frac{P_r}{P})(\frac{T}{T_r})(\frac{1+S/T_r}{1+S/T})$. S is the Sutherland constant of 110.4 K; T is the temperature in [K] and T_r is the reference temperature in [K].

Here, we give an example of the Cunningham slip correction C with the temperature of 25 °C and pressure of 101300 Pa. $f(D_p^*, \nu)$ curves are also shown with 1 through 4 charges respectively. It can be seen that when $\nu = 1$, the D_p^ν is equal to D_p^*. When $\nu > 1$, the D_p^ν is larger than D_p^*.

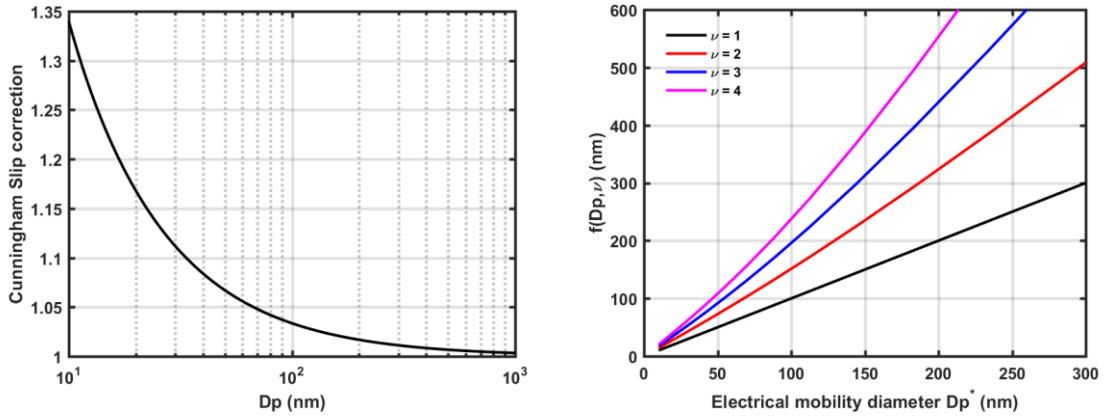

Fig.S4: Calculated Cunningham slip correction and f function curve.

Reference

ALBRECHT, B. A.: Aerosols, Cloud Microphysics, and Fractional Cloudiness, Science, 245, 1227-1230, 10.1126/science.245.4923.1227, 1989.

Bond, T. C., Doherty, S. J., Fahey, D. W., Forster, P. M., Berntsen, T., DeAngelo, B. J., Flanner, M. G., Ghan, S., Kärcher, B., Koch, D., Kinne, S., Kondo, Y., Quinn, P. K., Sarofim, M. C., Schultz, M. G., Schulz, M., Venkataraman, C., Zhang, H., Zhang, S., Bellouin, N., Guttikunda, S. K., Hopke, P. K., Jacobson, M. Z., Kaiser, J. W., Klimont, Z., Lohmann, U., Schwarz, J. P., Shindell, D., Storelvmo, T., Warren, S. G., and Zender, C. S.: Bounding the role of black carbon in the climate system: A scientific assessment, Journal of Geophysical Research: Atmospheres, 118, 5380-5552, 10.1002/jgrd.50171, 2013.

CHARLSON, R. J., SCHWARTZ, S. E., HALES, J. M., CESS, R. D., COAKLEY, J. A., HANSEN, J. E., and HOFMANN, D. J.: Climate Forcing by Anthropogenic Aerosols, Science, 255, 423-430, 10.1126/science.255.5043.423, 1992.

Chen, J., Zhao, C. S., Ma, N., Liu, P. F., Göbel, T., Hallbauer, E., Deng, Z. Z., Ran, L., Xu, W. Y., Liang, Z., Liu, H. J., Yan, P., Zhou, X. J., and Wiedensohler, A.: A parameterization of low visibilities for hazy days in the North China Plain, Atmospheric Chemistry and Physics, 12, 4935-4950, 10.5194/acp-12-4935-2012, 2012.

Ervens, B., Turpin, B. J., and Weber, R. J.: Secondary organic aerosol formation in cloud droplets and aqueous particles (aqSOA): a review of laboratory, field and model studies, Atmospheric Chemistry and Physics, 11, 11069-11102, 10.5194/acp-11-11069-2011, 2011.

Haywood, J., and Boucher, O.: Estimates of the direct and indirect radiative forcing due to tropospheric aerosols: A review, Reviews of Geophysics, 38, 513-543, 10.1029/1999rg000078, 2000.

Herrmann, H., Schaefer, T., Tilgner, A., Styler, S. A., Weller, C., Teich, M., and Otto, T.: Tropospheric aqueous-phase chemistry: kinetics, mechanisms, and its coupling to a changing gas phase, Chem Rev, 115, 4259-4334, 10.1021/cr500447k, 2015.

Heyder, J., Gebhart, J., Rudolf, G., Schiller, C. F., and Stahlhofen, W.: Deposition of particles in the human respiratory tract in the size range 0.005–15 µm, J Aerosol Sci, 17, 811-825, https://doi.org/10.1016/0021-8502(86)90035-2, 1986.

Löndahl, J., Massling, A., Pagels, J., Swietlicki, E., Vaclavik, E., and Loft, S.: Size-Resolved Respiratory-Tract Deposition of Fine and Ultrafine Hydrophobic and Hygroscopic Aerosol Particles During Rest and Exercise, Inhalation Toxicology, 19, 109-116, 10.1080/08958370601051677, 2007.

McFiggans, G., Artaxo, P., Baltensperger, U., Coe, H., Facchini, M. C., Feingold, G., Fuzzi, S., Gysel, M., Laaksonen, A., Lohmann, U., Mentel, T. F., Murphy, D. M., O'Dowd, C. D., Snider, J. R., and Weingartner, E.: The effect of physical and chemical aerosol properties on warm cloud droplet activation, Atmos. Chem. Phys., 6, 2593-2649, 10.5194/acp-6-2593-2006, 2006.

Shen, C., Zhao, G., Zhao, W., Tian, P., and Zhao, C.: Measurement report: Aerosol hygroscopic properties extended to 600 nm in the urban environment, Atmos. Chem. Phys. Discuss., 2020, 1-22, 10.5194/acp-2020-867, 2020.

Twomey, S.: Pollution and the planetary albedo, Atmospheric Environment (1967), 8, 1251-1256, http://dx.doi.org/10.1016/0004-6981(74)90004-3, 1974.

Wiedensohler, A., Lütkemeier, E., Feldpausch, M., and Helsper, C.: Investigation of the bipolar charge distribution at various gas conditions, Journal of Aerosol ence, 17, 413-416, 1986.

Wu, Z., Wang, Y., Tan, T., Zhu, Y., Li, M., Shang, D., Wang, H., Lu, K., Guo, S., Zeng, L., and Zhang, Y.: Aerosol Liquid Water Driven by Anthropogenic Inorganic Salts: Implying Its Key Role in Haze

Formation over the North China Plain, Environmental Science & Technology Letters, 5, 160-166, 10.1021/acs.estlett.8b00021, 2018.
Xu, W., Kuang, Y., Bian, Y., Liu, L., Li, F., Wang, Y., Xue, B., Luo, B., Huang, S., Yuan, B., Zhao, P., and Shao, M.: Current Challenges in Visibility Improvement in Southern China, Environmental Science & Technology Letters, 7, 395-401, 10.1021/acs.estlett.0c00274, 2020.

Effects of Multi-Charge on Aerosol Hygroscopicity Measurement by HTDMA

Chuanyang Shen[1], Gang Zhao[1,2], Chunsheng Zhao[1]

[1]Department of Atmospheric and Oceanic Sciences, School of Physics, Peking University, Beijing 100871, China
[2]College of Environmental Sciences and Engineering, Peking University, Beijing 100871, China

Correspondence to: Chunsheng Zhao (zcs@pku.edu.cn)

Abstract. The Humidified Tandem Differential Mobility Analyzer (HTDMA) is widely used to obtain ~~the~~submicron particles' hygroscopic properties ~~of submicron particles~~. Aerosol size-resolved hygroscopicity parameter κ measured by HTDMA will be influenced by the contribution of multiply charged aerosols, and this effect has seldom been discussed in previous field measurements. Our calculation demonstrates that the number ratio of multiply charged particles is quite considerable for some specific sizes between 100 nm and 300 nm, especially during the polluted episode. The multi charges will further lead to the ~~weakening~~compression effect of aerosol hygroscopicity in HTDMA measurements. Therefore, we propose a new algorithm to do the multi-charge correction for the size-resolved hygroscopicity κ considering both the ~~weakening~~compression effect and multi-charge number contribution. The application in field measurements shows that the relatively high hygroscopicity in the accumulation size range will lead to the overestimation of ~~the particle's~~particles' hygroscopicity smaller than 200 nm. The low hygroscopicity in coarse mode particles will lead to the underestimation of accumulation particles between 200 nm and 500 nm. The difference between corrected and measured κ can reach as large as 0.05, highlighting that special attention needs to be paid to the multi-charge effect when the HTDMA is used for the aerosol hygroscopicity measurement.

1 Introduction

Atmospheric particles can ~~affect the Earth-Atmosphere system through the interaction with~~scatter solar radiation~~,~~ and ~~acting as cloud nuclei~~absorb longwave radiation, imposing direct effects on the Earth's radiation balance (~~ALBRECHT, 1989; CHARLSON et al., 1992; Guo et al., 2017;~~ Haywood ~~&~~and Boucher, 2000; ~~Lohmann & Feichter, 2005 2001; Penner, Hegg, & Leaitch, 2001; Twomey, 1974~~Bond et al., 2013). They can also ~~impact human~~indirectly affect the climate through acting as cloud nuclei and modify the cloud optical properties and life ~~by degrading visibility and despairing respiratory health~~cycle ~~(Chang, Song, & Liu, 2009; Ibald-Mulli, Wichmann, Kreyling, & Peters, 2002; Su et al., 2017)~~(ALBRECHT, 1989;Twomey, 1974;CHARLSON et al., 1992)~~. All these effects are closely related to aerosol's hygroscopic property (Kreidenweis & Asa-Awuku, 2014), which reflects the aerosol's ability to absorb water under a specific relative humidity (RH).~~

. Both these two effects are closely related to aerosol particle's hygroscopicity, which describes the particle's ability to absorb water at sub or supersaturated conditions (e.g. McFiggans et al., 2006). Aerosol hygroscopicity also plays a vital role

in environmental aspects. It has been reported to be an important factor regulating environmental visibility because it can greatly enhance the particle's light scattering efficiency and degrade visibility under relatively high relative humidity (Chen et al., 2012;Xu et al., 2020). It can increase aerosol particle's liquid water content, affect the multiphase chemistry and local photochemistry, and facilitates particle formation and aging processes (Wu et al., 2018;Herrmann et al., 2015;Ervens et al., 2011). For human health, aerosol hygroscopicity directly determines the particle's size, thus modifying the deposition pattern of inhaled particles in the human respiratory tract (Heyder et al., 1986;Löndahl et al., 2007). In general, aerosol particle's hygroscopicity is one of the most important properties when quantifying the particle's climatic and environmental effects. It's also useful to characterize the particle's detailed chemical information. Therefore, it's necessary to offer a correct and detailed measurement of aerosol hygroscopicity.

Nowadays, ~~there are~~ many instruments ~~that~~ have been used to characterize aerosol particle's hygroscopicity, and HTDMA is one of the most widely used~~.~~ (Swietlicki et al., 2008;Tang et al., 2019;Kreidenweis and Asa-Awuku, 2014). As it can directly give the particle's size distribution after water uptake, it can be employed to ~~obtain both the mixing state and bulk mean hygroscopic properties of ambient aerosol particles (Swietlicki et al., 2017). Two Differential Mobility Analyzers (Swietlicki et al.)~~obtain both the mixing state and bulk mean hygroscopic properties of ambient aerosol particles. Two Differential Mobility Analyzers (Swietlicki et al., 2008) are used in this technique to quantify the size change of particles under different RH exposure. The measured distribution function (MDF) is skewed and smoothed from the particle's actual growth factor probability density function (GF-PDF). So several inversion algorithms have been developed to inverse the true GF-PDF (Cubison~~, Coe, & Gysel,~~ et al., 2005;~~–~~Gysel~~, McFiggans, & Coe,~~ et al., 2009;~~–~~Stolzenburg ~~&~~and McMurry, 2008; Voutilainen~~, Stratmann, & Kaipio,~~ et al., 2000). These inversions include the TDMAfit algorithm, the optimal estimation method (OEM~~)~~), and the TDMAinv algorithm. However, these algorithms are based on the assumption that the particles sampled are dominated by singly charged particles. Under this condition, the forward function can be simplified and data analysis is limited within the size concerned, not ~~interfered~~influenced by other sizes. If the number fraction of multiply charged particles at the selected dry diameter becomes significant, the measured results will be affected by the contributions from other dry sizes. In this case, appropriate data inversion is quite complicated.

However, in some special cases, the accurate data inversion for multi-charge particles can be achieved when the sampled particles are exclusively doubly or triply charged. ~~Duplissy et al. (2008) obtained the kernel functions for multiply charged particles and applied them in the data inversion to retrieve the correct GFs.~~Gysel et al. (2009) obtained the kernel functions for multiply charged particles and Duplissy et al. (2008) applied them in the data inversion to retrieve the correct growth factors (GFs). The dry sizes he selected are dominated by doubly or triply charged particles. However, in most field measurements, this assumption is invalid. As far as we are concerned, no previous studies have done the multi-charge correction for atmospheric aerosol particles in the HTDMA measurement. The effect of multi-charge correction on the size-resolved hygroscopicity is also not fully evaluated for atmospheric aerosols.

In this study, we first analyse the number contribution from particles carrying different charges. Then we present the ~~weakening~~compression effect of multiply charged particle's hygroscopicity in the HTDMA measurement. These two effects

were included into the algorithm to do the multi-charge correction for ~~particle's~~particles' size-resolved hygroscopicity. Then the application and corresponding influences of multi-charge correction on particle's hygroscopicity were discussed.

2 Multi-Charge Effects

2.1 Number Contribution from multiply charged particles

In the DMA sizing process ~~of the DMA~~, only particles within a narrow range of electrical mobility (Z_p) can transmit through the classifier exit slit and come to the downstream humidification and size distribution measurement system. The electrical mobility is defined as:

$$Z_p = \frac{\sout{neC(D_p)}}{\sout{3\pi\mu D_p}} \frac{veC(D_p)}{3\pi\mu D_p} \quad (1)$$

where $C(D_p)$ is the Cunningham slip correction; the e is elementary charge; the ~~n~~v is the number of elementary charges on the particle; the μ is the gas viscosity poise and D_p is the particle's physical diameter. From the equation ~~above,~~(1), we can see that with the same electrical mobility, particles can have different ~~combination~~combinations of diameters and number of charges, and this is where multi-charge effects come from.

The range that can pass through the DMA is defined as the mobility bandwidth, ΔZ_p:

$$\Delta Z_p = \frac{q_a}{q_{sh}} Z_p^* \quad (2)$$

where the Z_p^* is the set mobility, and the q_a and q_{sh} is the aerosol flow rate and sheath air flow rate, respectively. This equation doesn't account for diffusion broadening.

~~We can calculate the particle charge distribution at each size based on a theoretical model developed by Wiedensohler, Lütkemeier, Feldpausch, and Helsper (1986). Then the particle's probability to pass through a DMA classifier can be determined using the kernel function $G(i,x)$:~~

We can calculate the particle charge distribution at each size based on a theoretical model developed by Wiedensohler et al. (1986). Then the particle's probability to pass through a DMA classifier can be determined using the kernel function $G(D_p^*, x)$:

$$\sout{G(i,x)}(D_p^*, x) = \sout{\sum_{v=1}^{\infty} F(x,v)\Omega(x,v,i)} \quad \sout{(3)} \qquad \sum_{v=1}^{\infty} F(x,v)\Omega(x,v,D_p^*) \quad (3)$$

where the ~~i~~D_p^* is the diameter set in the DMA and x is the scale parameter; $F(x,v)$ is the charge distribution of particles that exit from a neutralizer~~.~~ with v charges at the scale parameter x. $\Omega(x,v,$~~i~~$)D_p^*)$ is the probability of particles to pass through the DMA ~~with v charges at~~when the ~~scale parameter x.~~set diameter is D_p^*. In this study, the maximum value of v is set as 10. Therefore, given a particle number size distribution ~~(PNSD~~n(x), the number of particles that can pass through the DMA with a set diameter of ~~i~~D_p^* is:

$$N(\sout{i) = \int_0^\infty G(i,x)\, D_p^*)} = \int_0^\infty G\left(D_p^*, x\right) n(x) dx \quad (4)$$

\sout{The}If the number of particles carrying specific charges is needed, the kernel function in the equation (4) need to be replaced with:

$$G_v\left(D_p^*, x\right) = F(x,v)\Omega(x,v,D_p^*) \quad (5)$$

and the corresponding number concentration of particle that can pass through the DMA is:

$$N_v(D_p^*) = \int_0^\infty G_v\left(D_p^*, x\right) n(x) dx \quad (6)$$

The number ratio of particles carrying different charges can \sout{also be determined.}be calculated from $N_v(D_p^*)/N(D_p^*)$.

Two aerosol size distribution cases representing \sout{the}a relatively clean period and a polluted period during our field measurement (refer to section 4) are shown in Fig. 1. The corresponding ratio of particles carrying different charges is calculated from the PNSD using the abovementioned DMA electrical mobility and charging theory. The detailed calculation procedures can be referred to in the supplement section 1. During the polluted period when total particle volume concentration is large, an obvious feature in PNSD is that the accumulation mode larger than 100 nm grows very large. The growth of this mode leads to an increase in the proportion of multi-charged particles, especially in the size range of 100-300 nm (electrical mobility diameter). For example, when we set 100 nm in the first DMA, more than 40% of the selected particles are multiply charged. This ratio is about 30% and 20% for the electrical diameter of 200 nm and 300 nm, respectively. Thus the HTDMA measured size-resolved hygroscopicity will also be influenced by those multiply charged large particles.

2.2 \sout{Weakening Effect}Compression effect of Hygroscopicity

In previous studies, Gysel et al. (2009) presented that the center of the kernel function at higher charges is systematically offset toward smaller GFs. An illustration figure (Fig.2) was shown to explain the cause of this compression effect. For electrical mobility diameter of 100 nm, the doubly and triply charged particles are about 151 nm and 196 nm, respectively. When all these three \sout{kind}kinds of particles have a true growth factor of 1.6, they will grow to the size of 160 nm, 242 nm, and 314 nm. Since the number of charges they carry \sout{remain}remains the same as before, their peak sizes in the second DMA are around 160 nm, 154 nm, and 150 nm. Therefore, the growth factors they display in the HTDMA measurement \sout{is}are 1.6, 1.54 and 1.5, respectively. It can be clearly seen that the growth factor is decreased or \sout{weakened}compressed. We call this phenomenon as \sout{weakening}the compression effect of growth factor or hygroscopicity brought by the multi-charge.

\sout{For each true growth factor, the HTDMA system will give a corresponding weakened growth factor, which can be calculated based on the electrical mobility theory (Fig. 2b). Each growth factor under a specific RH correspond to a hygroscopic parameter κ (Petters & Kreidenweis, 2007). Thus, the measured hygroscopicity is also weakened. As illustrated in Fig.3a, the weakening effect increases almost linearly with particle's hygroscopicity, with the slope as the weakening factor. For each}

~~electrical mobility diameter with different charges, a weakening factor of hygroscopicity can be calculated. The results are summarized in Fig.3b.~~

In the electrical mobility theory, when we set a diameter D_p^* in the DMA, the electrical mobility, Z_p, can be calculated as:

$$Z_p = \frac{eC(D_p^*)}{3\pi\mu D_p^*}. \quad (7)$$

Then the physical diameter (D_p^ν) of particles having the same electrical mobility but with ν charges is:

$$D_p^\nu = \frac{\nu eC(D_p^*)}{3\pi\mu Z_p} = \frac{C(D_p^\nu)}{C(D_p^*)}\nu D_p^* \quad (8)$$

and we define the f function as:

$$D_p^\nu = f(D_p^*, \nu). \quad (9)$$

The f function describes the physical diameter of multiply charged particles given an electrical mobility diameter. The properties and detailed calculation procedures of f function can be found in the supplement section 2.

For a particle of size D_p^ν with ν charges, if we assume a true growth factor of g_0, the particle will grow to the size of $g_0 D_p^\nu$. The virtual growth factor depicted in the DMA is expressed as g_{DMA}. These parameters will fit into this equation:

$$g_0 D_p^\nu = \mathrm{f}(g_{DMA} D_p^*, \nu) = g_0 f(D_p^*, \nu). \quad (10)$$

Given the f function, D_p^*, and ν, each g_0 can be substituted into the equation (10) to get a corresponding g_{DMA}. If $\nu = 1$, namely, particles carrying only one elementary charge, then g_{DMA} is equal to g_0. If $\nu > 1$, namely, particles are multiply charged, then the g_{DMA} will be lower than g_0. In Fig.2(b), an example is presented with $D_p^* = 100\ nm$ and $\nu = 2$. The X-axis is the assumed true growth factor (g_0) and the Y-axis is the calculated virtual growth factor depicted in DMA (g_{DMA}). Generally, the larger the g_0 is, the greater the difference between g_{DMA} and g_0 is.

According to Petters and Kreidenweis (2007), aerosol particle's hygroscopic parameter κ can be calculated from the growth factor under a specific RH using κ-kohler theory. As illustrated in Fig.3a, all the data points in Fig.2b can generate corresponding data points in the hygroscopicity space. It is clear that the decreased growth factor will result in a decreased hygroscopicity and the compression effect also increases almost linearly with the particle's hygroscopicity. If we fit these data points with a straight line across the origin, the slope can be considered as the compression factor. Fig.3a is an example for $D_p^* = 100\ nm\ and\ \nu = 2$. For each combination of electrical mobility diameter D_p^* and number of charges ν, we can repeat this calculation and linear fitting process, and obtain the compression factor $S(D_p^*, \nu)$ for hygroscopicity. The algorithm to calculate the compression factor is listed in Fig.4 and the results are summarized in Fig.3b and Table 1.

3 Method of Multi-Charge Correction

3.1 Multi-charge correction for size-resolved hygroscopicity

Multi-charge corrections are common when the DMA is used to scan the aerosol sizes, especially in the PNSD measurements. The shape of PNSD after multi-charge correction can be significantly different from that of the raw measured one. Therefore, it's necessary to evaluate the effect of multi-charge correction on the size-resolved hygroscopicity obtained by HTDMA. This study developed an algorithm to do the multi-charge correction for the measured values based on the work of Deng et al. (2011) and ~~Zhao et al. (2019).~~ Zhao et al. (2019)

Our correction is based on the assumption that, for each electrical mobility set at DMA1, the measured mean hygroscopicity is contributed by all particles that can pass through the DMA1. All the contributing particles carry the mean hygroscopicity of its physical size. For example, when a particle with a larger dry diameter ($\frac{n}{p}D_p^v$) carrying n charges pass through the DMA1 and make a contribution to the MDF, it's hard to tell which hygroscopicity it carries because it has a probability distribution function over hygroscopicity. In our algorithm, this particle is assumed to have a hygroscopicity of the mean value in the size $\frac{n}{p}D_p^v$. This assumption is statistically right and feasible but may not be true on a single-particle scale.

When the scan diameter in the first DMA is set as D_p^*, the observed mean hygroscopicity K^* by HTDMA can be expressed as:

~~$K_t = \frac{1}{N(i)}\int_0^\infty G^*(i,x)K^*(x)n(x)dx$~~ ~~(5)~~

~~where x is the scale parameter;~~ $K^*(D_p^*) = \frac{1}{N(D_p^*)}\int_0^\infty G_s(D_p^*,x)\mathrm{K}(x)n(x)dx$ (11)

where $\mathrm{K}(x)$ is the true mean κ for the scale parameter x; n(x) is the true aerosol number size distribution; ~~$N(i)$~~$N(D_p^*)$ is the total number concentration of particles that pass through the first DMA. The ~~$G^*(i,x)$~~$G_s(D_p^*,x)$ is the transformed kernel function ~~$G(i,x)$~~(D_p^*,x) of DMA1, which includes the ~~weakening~~compression effect $S(i,D_p^*,v)$.

~~$G^*(i,x)G_s(D_p^*,x) = \sum_{v=1}^{\infty} F(x,v)\Omega(x,v,i)S(i,v)\sum_{v=1}^{\infty} F(x,v)\Omega(x,v,D_p^*)S(D_p^*,v)$~~ (~~6~~12)

N(~~i~~) ~~$= \int_0^\infty G(i,x)$~~ $D_p^*) = \int_0^\infty G(D_p^*,x)\,n(x)dx$ (~~7~~13)

So the ~~question~~equation (5) can be simplified ~~as~~into the following:

~~$K_t = \int_0^\infty H(i,x)K^*(x)$~~ ~~(8)~~

~~or~~

~~$\mathbf{K = H}K^*(D_p^*) = \int_0^\infty H(D_p^*,x)\mathrm{K}(x)$~~ (14)

or

~~$\boldsymbol{K}^*$~~ ~~(9~~ ~~$= \mathbf{HK}$~~ (15)

where the ~~$K^*(x)$~~$\mathrm{K}(x)$ or ~~$\boldsymbol{K}^*\mathbf{K}$~~ is the true distribution of κ we want to obtain, and ~~$K_t K^*(D_p^*)$~~ or ~~$\mathbf{K}\boldsymbol{K}^*$~~ is the measured κ distribution. ~~$H(i,x)$~~(D_p^*,x) is:

$$H\text{~~(i,x)~~}\left(D_p^*, x\right) = \text{~~1~~}\frac{1}{\text{~~N(i)~~}N(D_p^*)}n(x)G^*\text{~~(i,x)~~}\left(D_p^*, x\right)dx \quad (\text{~~10~~}16)$$

$H\text{~~(i,x)~~}\left(D_p^*, x\right)$ or **H** matrix is the forward function and can be calculated from given information. Given a true κ distribution, we should be able to calculate the measured κ distribution imposed by multi-charge effect. The **H** matrix accounts for the DMA transfer function, the particle charge distribution, ~~weakening~~compression factors and number distribution of particles over each size parameter. The detailed steps to solve this matrix inverse problem can be found in ~~Zhao et al. (2019).~~Zhao et al. (2019)

One hypothetical uncorrected κ distribution $K^*(D_p^*)$ along with the corresponding multi-charge corrected ~~κ distributions~~$K(x)$ are shown in Fig.4. It represents a common case in the ambient environment: relatively low hygroscopicity for ultrafine particles, high hygroscopicity in accumulation mode size and nearly hydrophobic in the coarse mode. Two PNSD are used in the multi-charge correction, representing clean and pollution conditions. It can be seen that large variation of κ over sizes will cause large difference between pre- and post-corrected κ distribution, especially when the large variation exists in the singly, doubly and triply charged particle sizes. For example, the difference between measured and corrected κ reach a peak in 150 nm and 350 nm. For electrical mobility size of 150 nm, the corresponding doubly and triply charged particles are around 235 nm and 314 nm. These three sizes are located in the area where κ increases steeply. Similarly, for electrical mobility size of 350 nm, the corresponding doubly and triply charged particles are about 605 nm and 852 nm. These three sizes are also located in the area where κ drops greatly. Another point that can be seen from Fig. 4 is that an increasing trend of κ will cause the measured κ overestimated and a decreasing trend of κ will cause the measured κ underestimated.

3.2 Multi-charge correction for mixing state

Except for the size-resolved mean hygroscopicity, the key information that can be obtained from the HTDMA also includes the mixing state and the detailed shape of GF-PDF or κ-PDF. The correction of GF-PDF or κ-PDF involves the inversion of two-dimensional vectors, which is too complicated for this study. But the mixing state can be simply represented by the particle number fraction in different GF ranges. Here, we can use the number fraction of Less-Hygroscopic particles as an example.

The correction for mixing state is similar in general to the correction for mean hygroscopicity, but differ in some minor aspects. When the scan diameter in DMA is set as ~~D_t~~D_p^*, the observed number fraction of less-hygroscopic particles by HTDMA can be expressed as:

$$\text{~~$A_t = \frac{1}{N(i)}\int_0^\infty G^*(i,x)A^*(x)n(x)dx$~~}\ M^*(D_p^*) = \frac{1}{N(D_p^*)}\int_0^\infty G_s\left(D_p^*, x\right)M(x)n(x)dx \quad (\text{~~11~~}17)$$

where the ~~$A_t M^*(D_p^*)$~~ is the measured number fraction of LH group particles at the DMA selected diameter ~~D_t~~D_p^*, the ~~$A^*(x)$~~$M(x)$ represents the true number fraction at scale parameter x.

~~$G^*(i,x)G_s(D_p^*,x) = \sum_{v=1}^{\infty} F(x,v)\Omega(x,v,i)\,C(i,x)$~~ ~~(12~~ $\sum_{v=1}^{\infty} F(x,v)\Omega(x,v,D_p^*)\,S_M(D_p^*,v)$ (18)

N(~~i~~) ~~$= \int_0^{\infty} G(i,x)\,D_p^*)$~~ $= \int_0^{\infty} G(D_p^*,x)\,n(x)dx$ (~~13~~19)

where the ~~$C(i,x)S_M(D_p^*,v)$~~ represents the correction factor caused by the ~~weakening~~compression effect. This factor varies with different GF-probability distribution function (GF-PDF) and cannot be simplified into a constant. If we assume that the ~~weakening~~compression effect on the LH number ratio can be neglected, then this parameter is 1 and the ~~question~~equation can be simplified into:

~~$A_i = \int_0^{\infty} H(i,x)A^*(x)$~~ ~~(14)~~

~~or~~

~~**$\mathbf{A = HA^*}$**~~ ~~(15~~ $M^*(D_p^*) = \int_0^{\infty} H(D_p^*,x)M(x)$ (20)

or

$\boldsymbol{M^* = HM}$ (21)

where ~~$H(i,x)(D_p^*,x)$~~ is:

H~~(i,x)~~$(D_p^*,x) = \frac{1}{N(i)}\frac{1}{N(D_p^*)}n(x)G(i,D_p^*,x)$dx (~~16~~22)

The ~~$H(i,x)(D_p^*,x)$~~ or the **H** matrix can also be calculated from given information. One hypothetical ~~A(x)~~measured $M^*(D_p^*)$ distributions along with the corresponding multi-charge corrected ~~A(x)~~$M(x)$ distributions are also shown in Fig.~~4~~5.

4 Application in field measurements

During the winter of 2019, a comprehensive aerosol field measurement focusing on hygroscopicity properties over a size range of 50-600 nm was conducted at a Beijing urban site. The measurement was conducted on the rooftop of a six-floor building in the campus of Peking University. It shares the same location with the AERONET station of BEIJING_PKU (39°59' N, 116°18' E). The sampling site is in the northwest of Beijing, surrounded by schools, residential buildings, and shopping centers.

During the measurement, an HTDMA instrument was employed to measure hygroscopic growth factors of particles with dry ~~diameter of 50, 100, 200, 300, 400, 500, and 600 nm at 85% RH. Particle number size distributions (PNSD) were also measured by a BMI scanning electrical mobility sizer (BMI SEMS, Model 2100) with a size range of 10–1000 nm. In the measurement, a PM10 impactor was used to remove particles with aerodynamic diameter larger than 10 μm.~~diameters of 50, 100, 200, 300, 400, 500, and 600 nm at 85% RH. Before the aerosol sampling, a PM10 impactor was used to remove aerosol particles with aerodynamic diameters larger than 10 μm. Then a dryer was used to decrease the RH to less than 30%. Next, the dried poly-disperse particles were guided into a splitter with different instruments located downstream. These instruments include the HTDMA and a BMI scanning electrical mobility sizer (BMI SEMS, Model 2100). In both these two

measurement systems, aerosol particles were firstly charged by a soft X-ray neutralizer (TSI, Model 3088) and those negatively charged particles were selected by the DMA. For the HTDMA, the ratio of sample to sheath in the first DMA is 0.75/4. To calibrate the measurement system, ammonium sulfate particles were tested to compare with the theoretical values. The calibration includes both the dry test and RH test. For the best working performance, the room was air-conditioned at 25℃ and circulated all the time. Particle number size distributions (PNSD) were given by the SEMS with a size range of 10-1000 nm.

To evaluate the effects of multiply charged particles on the size-resolved hygroscopicity, we choose two weeks' measurement data to do the multi charge correction. The particle number size distribution and measured size-resolved hygroscopicity κ are shown in Fig. 6. For better comparison, we also present the size-resolved difference between measured and corrected hygroscopicity data. What's to be noted is that, since the upper limit of hygroscopicity measurement is 600 nm, the hygroscopicity in the higher size range is assumed to decrease linearly to 0 at 1 μm. Here we presume the hygroscopicity for coarse mode particles is 0. For particles larger than 1 μm, the number concentration is also assumed to decrease linearly to 0 at 1.2 μm in the multi-charge correction.

Generally, for particles less than 200 nm, the particle's hygroscopicity will be overestimated. For particles larger than 200 nm, the particle's hygroscopicity will be underestimated. From Fig. 6(b), we can see that in the urban environment, the hygroscopicity often peaks at the size range of 200-400 nm. The relatively high hygroscopicity in this size range will be mixed into the ~~lower~~smaller size in the HTDMA measurement, leading to a false increase of measured κ. Similarly, most of the ambient particles have a relatively lower hygroscopicity in the upper size. When they carry multiple charges and sneak into to the lower accumulation size set by the DMA, the hygroscopicity in the target size region will be lowered.

The overall difference between corrected and measured size-resolved κ mostly lie within 0.05. For the electrical mobility size that affected most by multi-charge particles, e.g. 100 nm, the doubly or triply charged particles correspond to 151 nm and 196 nm. These three sizes normally share similar hygroscopicity, which leads to a small effect on the measured κ. However, when there exists a large variation of hygroscopicity in these three sizes, the multi-charge correction in this size will be necessary. For particles larger than 300 nm, the multi-charge effect is mostly contributed by particles larger than 500 nm. Few field observations on hygroscopicity have covered this size range, which brought large uncertainty to the multi-charge correction. From our measurement, the variation of hygroscopicity in this size range is relatively large, depending on different pollution conditions~~.~~ (Shen et al., 2020). On average, the hygroscopicity of particles above 500 nm is lower than other accumulation sizes. Because of the assumption of few particles above 1 um, the multi-charge effect on the size above 500 nm is fairly small. In practice, this can be achieved by installing an impactor before the inlet of the first DMA.

5 Conclusion

The HTDMA instrument has been extensively used in numerous field measurements to obtain the hygroscopic properties of submicron particles. Aerosol particles sampled by the DMA are quasi-monodisperse with different charges and different

diameters. Thus, size-resolved hygroscopicity measured by DMA will be influenced by the contribution of multiply charged aerosols. In the hygroscopicity measurement by HTDMA, this effect has seldom been discussed in previous field measurements.

In this study, we ~~firstly~~first demonstrate that the multi-charge not only influence the hygroscopicity measurement through the number contribution, but also through the ~~weakening~~compression effect. On one hand, the number fraction of multiply charged particles is quite considerable, especially under polluted conditions. Results show that there can be 30% to 40% of selected particles are mistaken from large multiply charged particles in the polluted period. On the other hand, the growth factor or hygroscopicity measured by the HTDMA can be smaller than the true value for multiply charged particles, which is also called the multi-charge ~~weakening~~compression effect. This effect can be quantified as a ~~weakening~~compression factor using the electrical mobility theory. The ~~weakening~~compression factor reaches its peak around the size of 200 nm and increases with the number of charges the particle carries.

We propose an algorithm to do the multi-charge correction for the size-resolved hygroscopicity κ and mixing state. The algorithm is based on the principle of SMPS multi-charge correction and the knowledge of aerosol PNSD is required. The key in this algorithm is to obtain the forward function and to solve the inverse problem.

The proposed multi-charge correction is applied in a field measurement to evaluate the multi-charge effects. The relatively high hygroscopicity in accumulation size range will lead to overestimation of the particle's hygroscopicity smaller than 200 nm. The low hygroscopicity in coarse mode particles will lead to the underestimation of accumulation particles. The difference between measured and corrected κ can reach as large as 0.05.

The measured hygroscopicity between 200 nm and 400 nm is influenced by multiply charged particles larger than 400 nm, indicating that the hygroscopic measurement above 400 nm is necessary if correct hygroscopic properties want to be obtained for accumulation mode particles. For particles larger than 400 nm, the multi-charge effect can be removed by installing an impactor with cutting size around 1 μm or even lower. In the future hygroscopicity measurements, our studies highlight that special attention should be paid to the multi-charge effects, and multi-charge correction should be done if accurate size-resolved hygroscopicity needs to be obtained.

Competing interests. The authors declare that they have no conflict of interest.

Data availability. The data used in this study is available when requesting the authors.

Author contributions. Chuanyang Shen, Gang Zhao and Chunsheng Zhao discussed the results; Chuanyang Shen wrote the manuscript.

Acknowledgements. This work is supported by the National Natural Science Foundation of China (41590872).

References

ALBRECHT, B. A. (1989). Aerosols, Cloud Microphysics, and Fractional Cloudiness. *Science*, *245*(4923), 1227-1230. doi:10.1126/science.245.4923.1227

Chang, D., Song, Y., & Liu, B. (2009). Visibility trends in six megacities in China 1973–2007. *Atmospheric Research*, *94*(2), 161-167. doi:10.1016/j.atmosres.2009.05.006

CHARLSON, R. J., SCHWARTZ, S. E., HALES, J. M., CESS, R. D., COAKLEY, J. A., HANSEN, J. E., & HOFMANN, D. J. (1992). Climate Forcing by Anthropogenic Aerosols. *Science*, *255*(5043), 423-430. doi:10.1126/science.255.5043.423

Cubison, M. J., Coe, H., & Gysel, M. (2005). A modified hygroscopic tandem DMA and a data retrieval method based on optimal estimation. *Journal of Aerosol Science*, *36*(7), 846-865. doi:10.1016/j.jaerosci.2004.11.009

Deng, Z. Z., Zhao, C. S., Ma, N., Liu, P. F., Ran, L., Xu, W. Y., . . . Wiedensohler, A. (2011). Size-resolved and bulk activation properties of aerosols in the North China Plain. *Atmospheric Chemistry and Physics*, *11*(8), 3835-3846. doi:10.5194/acp-11-3835-2011

Duplissy, J., Gysel, M., Alfarra, M. R., Dommen, J., Metzger, A., Prevot, A. S. H., . . . Baltensperger, U. (2008). Cloud forming potential of secondary organic aerosol under near atmospheric conditions. *Geophysical Research Letters*, *35*(3). doi:10.1029/2007gl031075

Guo, Jianping, Su, Tianning, Li, Zhanqing, . . . Liu. (2017). Declining frequency of summertime local-scale precipitation over eastern China from 1970-to-2010 and its potential link to aerosols. *Geophysical Research Letters*.

Gysel, M., McFiggans, G. B., & Coe, H. (2009). Inversion of tandem differential mobility analyser (TDMA) measurements. *Journal of Aerosol Science*, *40*(2), 134-151. doi:10.1016/j.jaerosci.2008.07.013

Haywood, J., & Boucher, O. (2000). Estimates of the direct and indirect radiative forcing due to tropospheric aerosols: A review. *Reviews of Geophysics*, *38*(4), 513-543. doi:10.1029/1999rg000078

Ibald-Mulli, A., Wichmann, H. E., Kreyling, W., & Peters, A. (2002). Epidemiological Evidence on Health Effects of Ultrafine Particles. *Journal of Aerosol Medicine*, *15*(2), 189-201. doi:10.1089/089426802320282310

Kreidenweis, S. M., & Asa-Awuku, A. (2014). Aerosol Hygroscopicity: Particle Water Content and Its Role in Atmospheric Processes. 331-361. doi:10.1016/b978-0-08-095975-7.00418-6

Lohmann, U., & Feichter, J. (2005). Global indirect aerosol effects: a review. *Atmos. Chem. Phys.*, *5*(3), 715-737. doi:10.5194/acp-5-715-2005

Penner, J. E., Hegg, D., & Leaitch, R. (2001). Unraveling the role of aerosols in climate change. *Environmental Science & Technology*, *35*(15), 332A-340A. doi:10.1021/es0124414

Petters, M., & Kreidenweis, S. (2007). A single parameter representation of hygroscopic growth and cloud condensation nucleus activity. *Atmospheric Chemistry and Physics*, *7*(8), 1961-1971.

Stolzenburg, M. R., & McMurry, P. H. (2008). Equations Governing Single and Tandem DMA Configurations and a New Lognormal Approximation to the Transfer Function. *Aerosol Science and Technology*, *42*(6), 421-432. doi:10.1080/02786820802157823

Su, T., Li, J., Li, C., Kai Hon Lau, A., Yang, D., & Shen, C. (2017). An intercomparison of AOD-converted PM2.5 concentrations using different approaches for estimating aerosol vertical distribution. *Atmospheric Environment*, 531-542.

Swietlicki, E., Hansson, H. C., Hämeri, K., Svenningsson, B., Massling, A., McFiggans, G., . . . Kulmala, M. (2017). Hygroscopic properties of submicrometer atmospheric aerosol particles measured with H-TDMA instruments in various environments—a review. *Tellus B: Chemical and Physical Meteorology*, *60*(3), 432-469. doi:10.1111/j.1600-0889.2008.00350.x

Twomey, S. (1974). Pollution and the planetary albedo. *Atmospheric Environment (1967)*, *8*(12), 1251-1256. doi:http://dx.doi.org/10.1016/0004-6981(74)90004-3

Voutilainen, A., Stratmann, F., & Kaipio, J. P. (2000). A NON-HOMOGENEOUS REGULARIZATION METHOD FOR THE ESTIMATION OF NARROW AEROSOL SIZE DISTRIBUTIONS. *Journal of Aerosol Science*, *31*(12), 1433-1445. doi:https://doi.org/10.1016/S0021-8502(00)00044-6

Wiedensohler, A., Lütkemeier, E., Feldpausch, M., & Helsper, C. (1986). Investigation of the bipolar charge distribution at various gas conditions. *Journal of Aerosol ence*, *17*(3), 413-416.

~~Zhao, G., Tao, J., Kuang, Y., Shen, C., Yu, Y., & Zhao, C. (2019). Role of black carbon mass size distribution in the direct aerosol radiative forcing. *Atmospheric Chemistry and Physics*, *19*(20), 13175-13188. doi:10.5194/acp-19-13175-2019~~

Table 1 The ~~weakening~~compression factor ~~of~~for aerosol particle's hygroscopicity under 85% RH over different electrical mobility diameters.

Dp (nm) / N	50	100	200	300	400	500	600
1	1	1	1	1	1	1	1
2	0.98	0.90	0.85	0.86	0.87	0.89	0.90
3	0.95	0.82	0.77	0.80	0.83	0.85	0.86
4	0.92	0.77	0.73	0.77	0.80	0.82	0.84
5	0.89	0.74	0.71	0.75	0.78	0.81	0.83

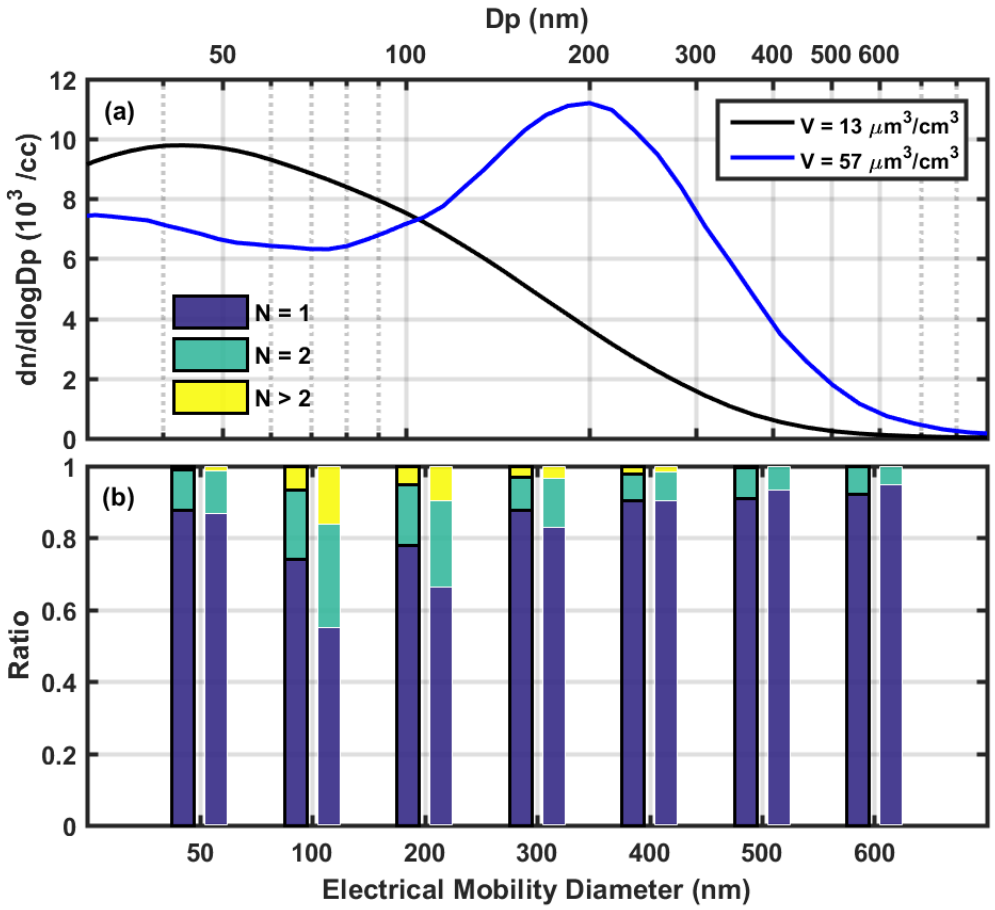

Dp (nm) / ν	50	100	200	300	400	500	600
1	1	1	1	1	1	1	1
2	0.98	0.90	0.85	0.86	0.87	0.89	0.90
3	0.95	0.82	0.77	0.80	0.83	0.85	0.86
4	0.92	0.77	0.73	0.77	0.80	0.82	0.84
5	0.89	0.74	0.71	0.75	0.78	0.81	0.83

375

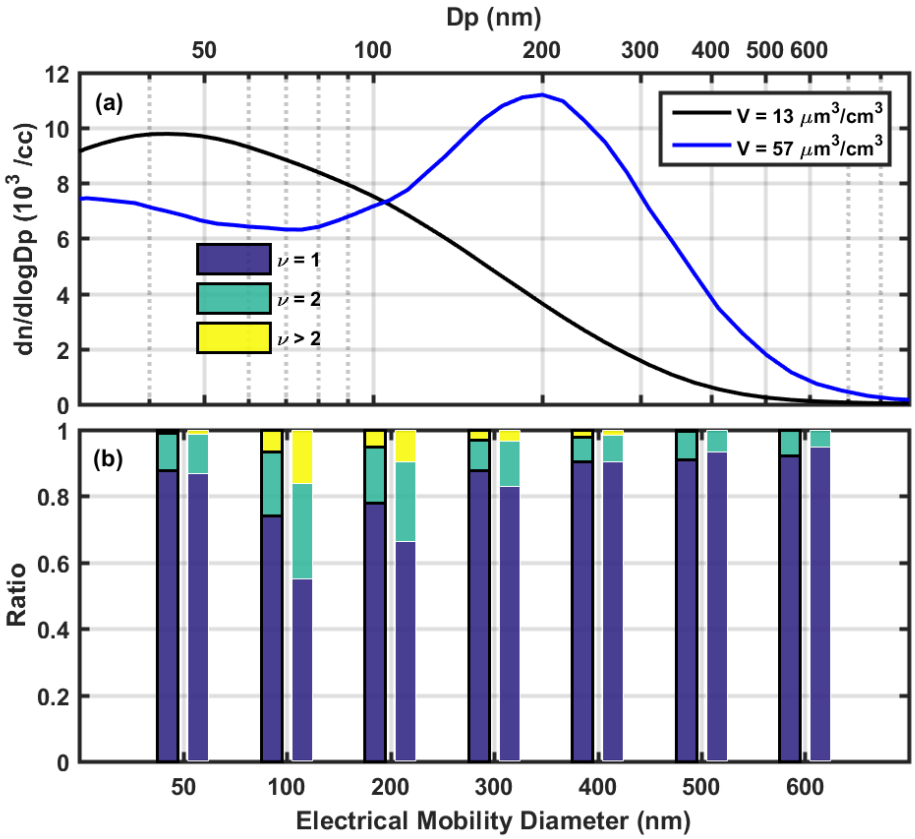

Figure 1. (a) Two cases of particle number size distribution during the field measurement. The black line represents the relatively clean period and the blue line represents the heavily polluted period. (b) The number ratio of particles carrying different charges. The left bar with black edge color corresponds to the PNSD in black line; the right bar without edge color corresponds to the PNSD in blue line.

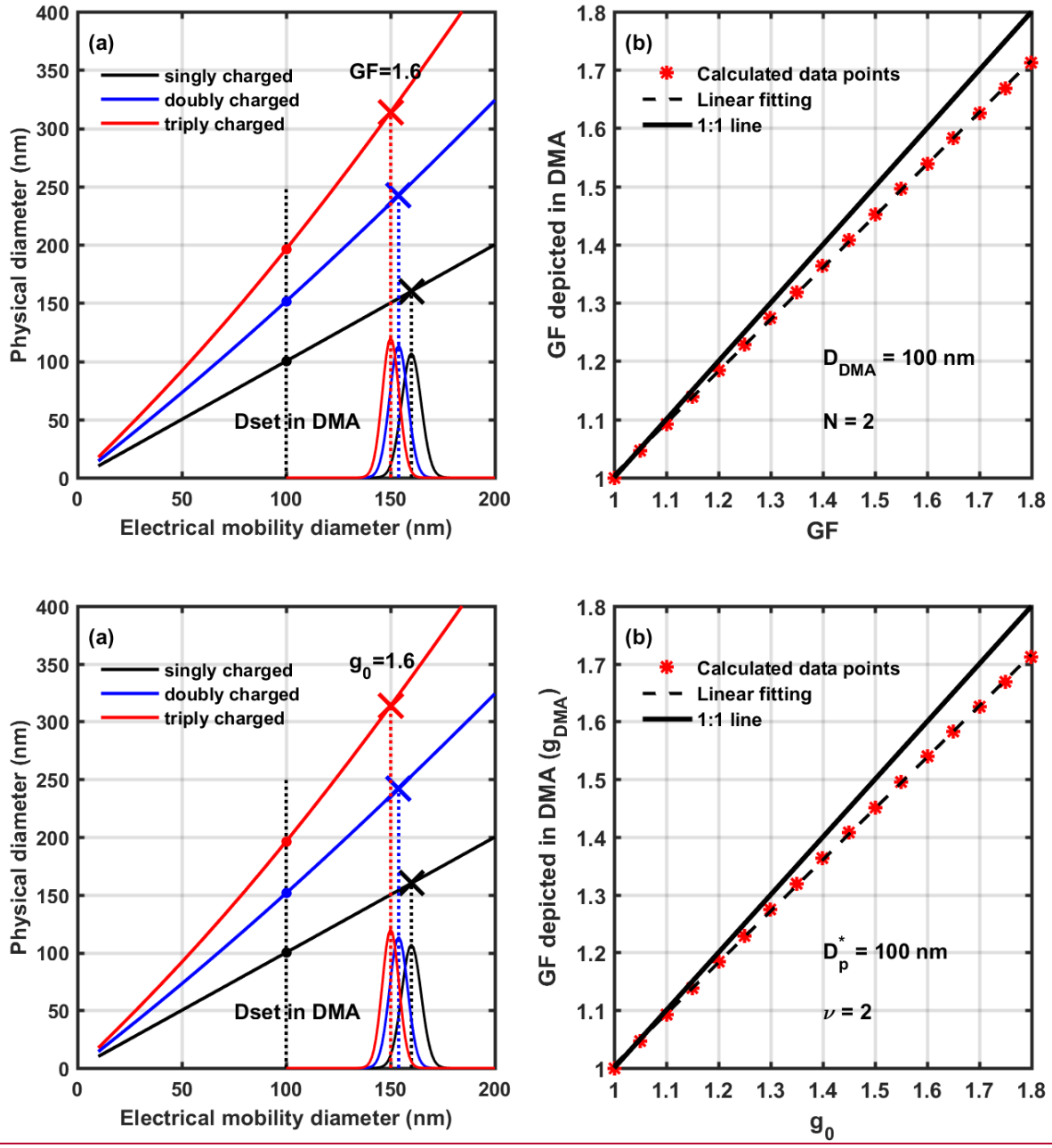

Figure 2. (a) Effects of particle carrying multiple charges; black, blue and red lines represent singly, doubly and triply charges particles, respectively. The circle points are particles selected by DMA when the electrical mobility diameter is set as 100 nm. When the true growth factor is 1.6, these particles will grow to the corresponding crossed points. The mode of the MDF of multiply charged particles peaks at a smaller GF than the true value. (b) The ~~weakening~~compression effect of different growth factors for doubly charged particles with an electrical diameter of 100 nm.

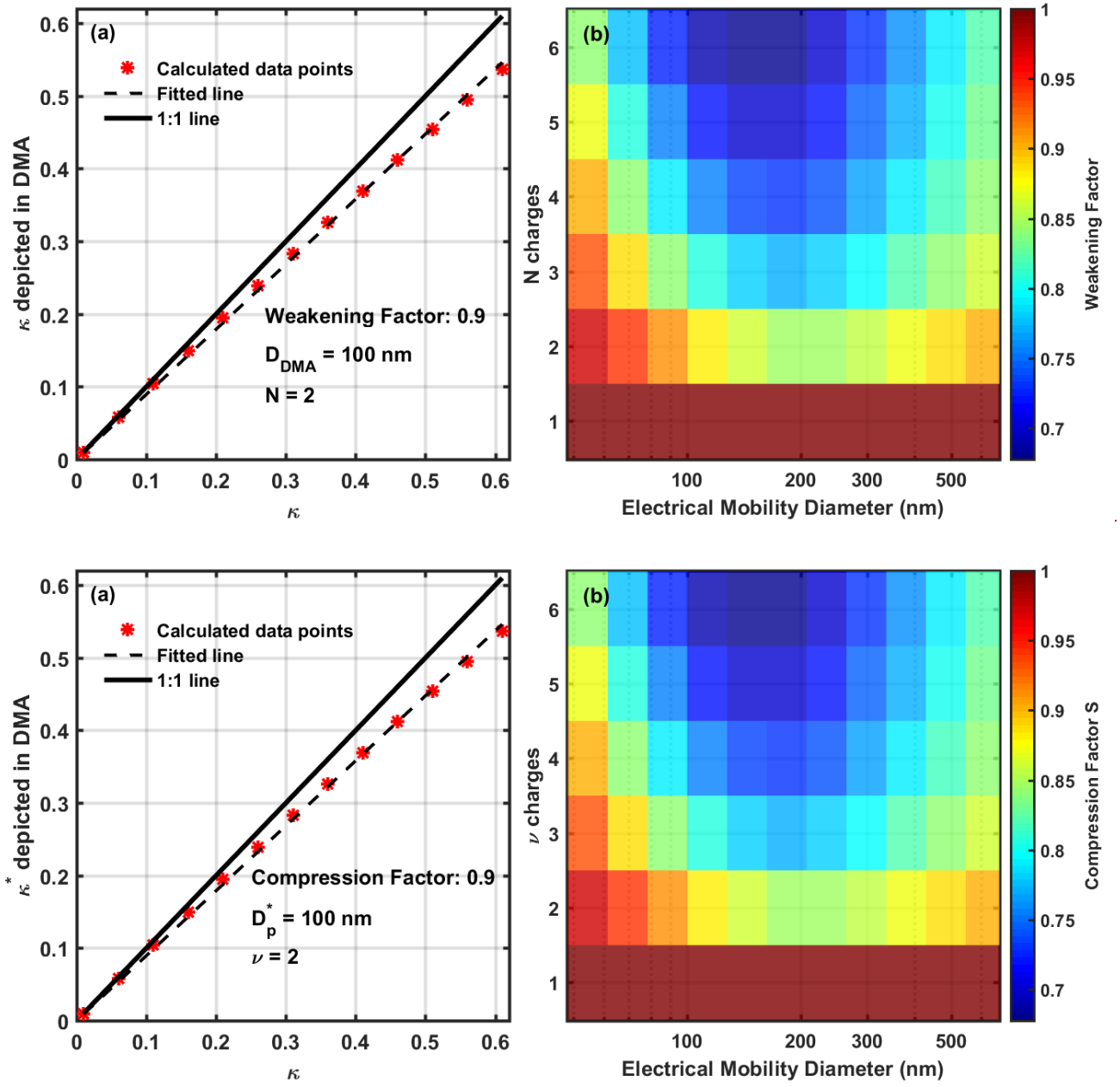

Figure 3. (a) The ~~weakening~~compression effect of different hygroscopicity (under 85% RH) for doubly charged particles with an electrical mobility diameter of 100 nm. The fitted slope or ~~weakening~~compression factor is 0.8953. (b) A summary of ~~weakening~~compression factors for different electrical mobility diameters carrying different number of charges at 85% RH.

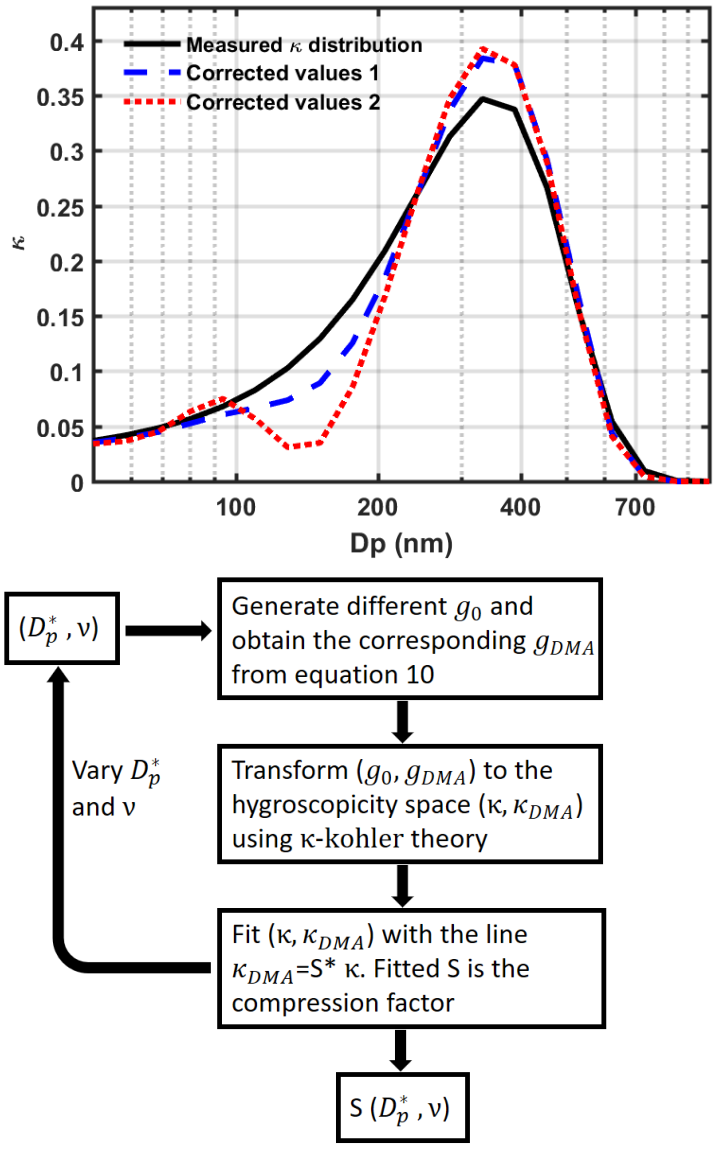

Figure 4. The algorithm procedures to calculate the compression factor.

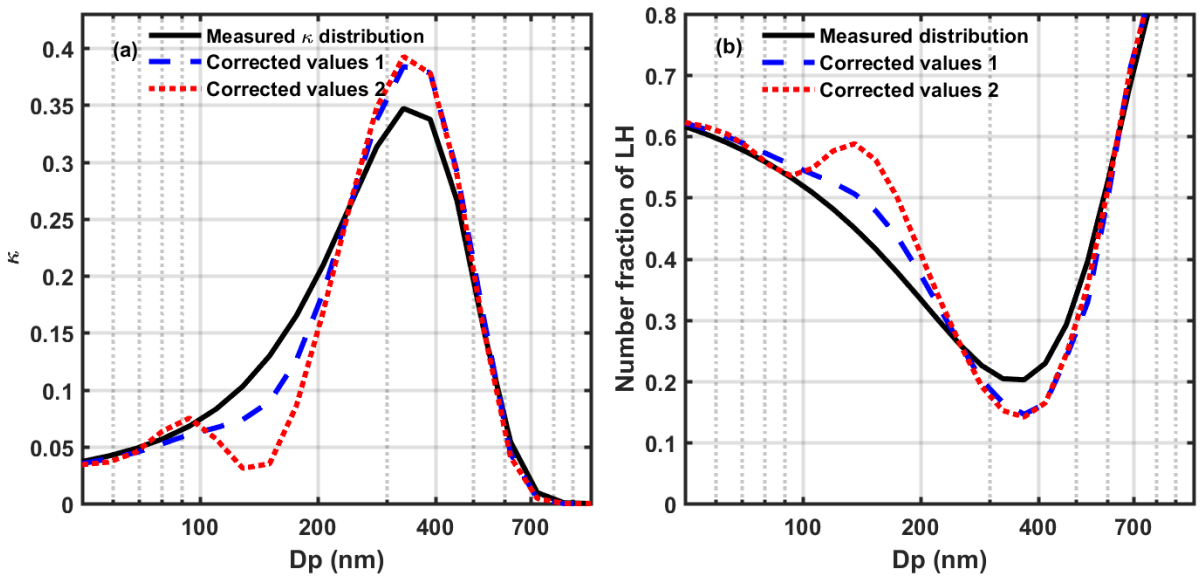

Figure 5. (a) Multi-charge correction for ~~a~~one hypothetical measured κ distribution. The black line is the measured size-resolved κ and the dashed lines are the multi-charge corrected κ distributions based on different number size distributions. The used PNSD can be referred to in Fig. 1.

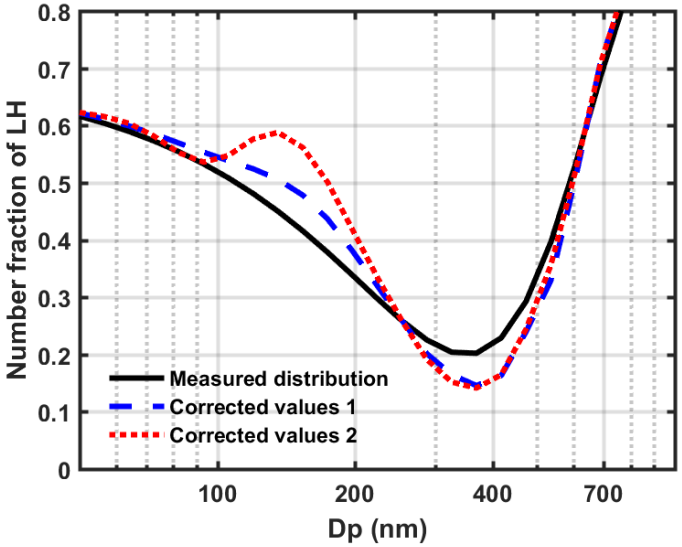

(b)~~Figure 5.~~ Multi-charge correction for one ~~hypothetical~~ mixing state distribution. The black lines are the measured size-resolved number fraction of LH and the dashed lines are the multi-charge corrected values based on different number size distributions.

415

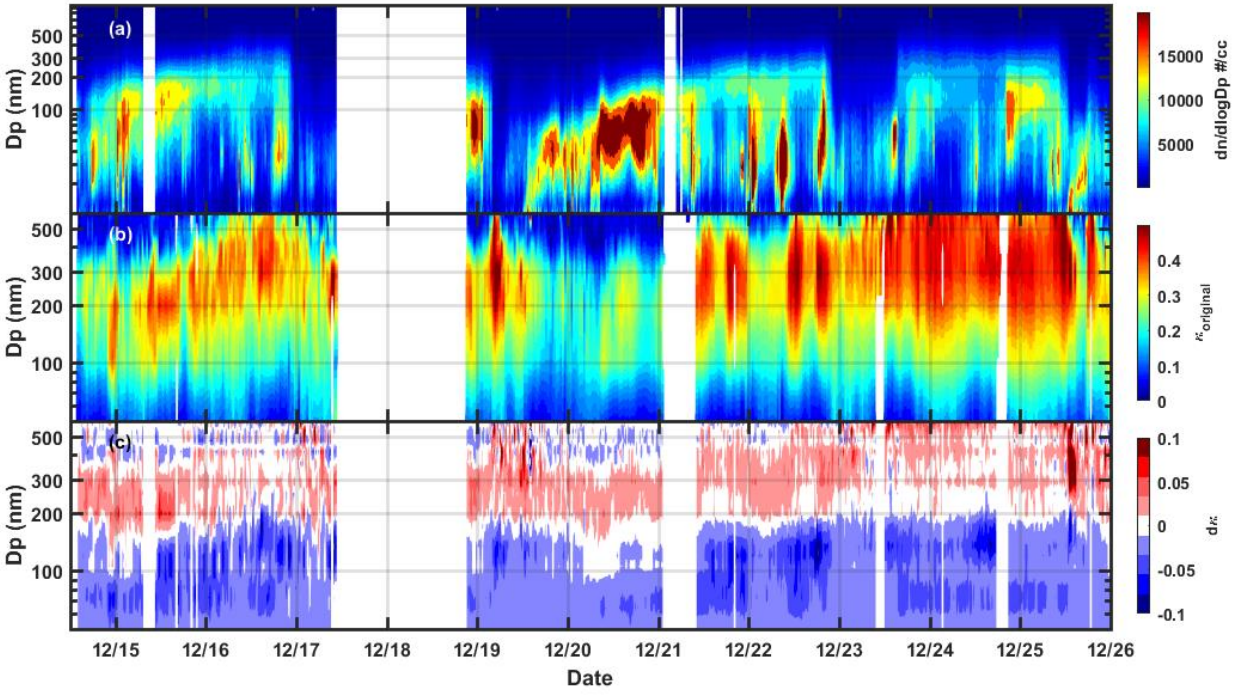

Figure 6. The field measurement of the PNSD and size-resolved hygroscopicity in Beijing winter. (a)The filled color gives the particle number concentration over different diameter (Dp). (b)The filled color represent the size-resolved hygroscopicity parameter κ. (c) The difference between measured and multi-charge corrected κ. $d_\kappa = \kappa_{corrected} - \kappa_{measured}$.

420

References

ALBRECHT, B. A.: Aerosols, Cloud Microphysics, and Fractional Cloudiness, Science, 245, 1227-1230, 10.1126/science.245.4923.1227, 1989.

Bond, T. C., Doherty, S. J., Fahey, D. W., Forster, P. M., Berntsen, T., DeAngelo, B. J., Flanner, M. G., Ghan, S., Kärcher, B., Koch, D., Kinne, S., Kondo, Y., Quinn, P. K., Sarofim, M. C., Schultz, M. G., Schulz, M., Venkataraman, C., Zhang, H., Zhang, S., Bellouin, N., Guttikunda, S. K., Hopke, P. K., Jacobson, M. Z., Kaiser, J. W., Klimont, Z., Lohmann, U., Schwarz, J. P., Shindell, D., Storelvmo, T., Warren, S. G., and Zender, C. S.: Bounding the role of black carbon in the climate system: A scientific assessment, Journal of Geophysical Research: Atmospheres, 118, 5380-5552, 10.1002/jgrd.50171, 2013.

CHARLSON, R. J., SCHWARTZ, S. E., HALES, J. M., CESS, R. D., COAKLEY, J. A., HANSEN, J. E., and HOFMANN, D. J.: Climate Forcing by Anthropogenic Aerosols, Science, 255, 423-430, 10.1126/science.255.5043.423, 1992.

Chen, J., Zhao, C. S., Ma, N., Liu, P. F., Göbel, T., Hallbauer, E., Deng, Z. Z., Ran, L., Xu, W. Y., Liang, Z., Liu, H. J., Yan, P., Zhou, X. J., and Wiedensohler, A.: A parameterization of low visibilities for hazy days in the North China Plain, Atmospheric Chemistry and Physics, 12, 4935-4950, 10.5194/acp-12-4935-2012, 2012.

Cubison, M. J., Coe, H., and Gysel, M.: A modified hygroscopic tandem DMA and a data retrieval method based on optimal estimation, J Aerosol Sci, 36, 846-865, 10.1016/j.jaerosci.2004.11.009, 2005.

Deng, Z. Z., Zhao, C. S., Ma, N., Liu, P. F., Ran, L., Xu, W. Y., Chen, J., Liang, Z., Liang, S., Huang, M. Y., Ma, X. C., Zhang, Q., Quan, J. N., Yan, P., Henning, S., Mildenberger, K., Sommerhage, E., Schafer, M., Stratmann, F., and Wiedensohler, A.: Size-resolved and bulk activation properties of aerosols in the North China Plain, Atmospheric Chemistry and Physics, 11, 3835-3846, 10.5194/acp-11-3835-2011, 2011.

Duplissy, J., Gysel, M., Alfarra, M. R., Dommen, J., Metzger, A., Prevot, A. S. H., Weingartner, E., Laaksonen, A., Raatikainen, T., Good, N., Turner, S. F., McFiggans, G., and Baltensperger, U.: Cloud forming potential of secondary organic aerosol under near atmospheric conditions, Geophys Res Lett, 35, 10.1029/2007gl031075, 2008.

Ervens, B., Turpin, B. J., and Weber, R. J.: Secondary organic aerosol formation in cloud droplets and aqueous particles (aqSOA): a review of laboratory, field and model studies, Atmospheric Chemistry and Physics, 11, 11069-11102, 10.5194/acp-11-11069-2011, 2011.

Fierce, L., Onasch, T. B., Cappa, C. D., Mazzoleni, C., China, S., Bhandari, J., Davidovits, P., Fischer, D. A., Helgestad, T., Lambe, A. T., Sedlacek, A. J., 3rd, Smith, G. D., and Wolff, L.: Radiative absorption enhancements by black carbon controlled by particle-to-particle heterogeneity in composition, Proc Natl Acad Sci U S A, 117, 5196-5203, 10.1073/pnas.1919723117, 2020.

Gysel, M., McFiggans, G. B., and Coe, H.: Inversion of tandem differential mobility analyser (TDMA) measurements, J Aerosol Sci, 40, 134-151, 10.1016/j.jaerosci.2008.07.013, 2009.

Haywood, J., and Boucher, O.: Estimates of the direct and indirect radiative forcing due to tropospheric aerosols: A review, Reviews of Geophysics, 38, 513-543, 10.1029/1999rg000078, 2000.

Herrmann, H., Schaefer, T., Tilgner, A., Styler, S. A., Weller, C., Teich, M., and Otto, T.: Tropospheric aqueous-phase chemistry: kinetics, mechanisms, and its coupling to a changing gas phase, Chem Rev, 115, 4259-4334, 10.1021/cr500447k, 2015.

Heyder, J., Gebhart, J., Rudolf, G., Schiller, C. F., and Stahlhofen, W.: Deposition of particles in the human respiratory tract in the size range 0.005–15 µm, J Aerosol Sci, 17, 811-825, https://doi.org/10.1016/0021-8502(86)90035-2, 1986.

Kreidenweis, S. M., and Asa-Awuku, A.: Aerosol Hygroscopicity: Particle Water Content and Its Role in Atmospheric Processes, 331-361, 10.1016/b978-0-08-095975-7.00418-6, 2014.

Löndahl, J., Massling, A., Pagels, J., Swietlicki, E., Vaclavik, E., and Loft, S.: Size-Resolved Respiratory-Tract Deposition of Fine and Ultrafine Hydrophobic and Hygroscopic Aerosol Particles During Rest and Exercise, Inhalation Toxicology, 19, 109-116, 10.1080/08958370601051677, 2007.

McFiggans, G., Artaxo, P., Baltensperger, U., Coe, H., Facchini, M. C., Feingold, G., Fuzzi, S., Gysel, M., Laaksonen, A., Lohmann, U., Mentel, T. F., Murphy, D. M., O'Dowd, C. D., Snider, J. R., and Weingartner, E.: The effect of physical and chemical aerosol properties on warm cloud droplet activation, Atmos. Chem. Phys., 6, 2593-2649, 10.5194/acp-6-2593-2006, 2006.

Petters, M., and Kreidenweis, S.: A single parameter representation of hygroscopic growth and cloud condensation nucleus activity, 2007.

Shen, C., Zhao, G., Zhao, W., Tian, P., and Zhao, C.: Measurement report: Aerosol hygroscopic properties extended to 600 nm in the urban environment, Atmos. Chem. Phys. Discuss., 2020, 1-22, 10.5194/acp-2020-867, 2020.

Stolzenburg, M. R., and McMurry, P. H.: Equations Governing Single and Tandem DMA Configurations and a New Lognormal Approximation to the Transfer Function, Aerosol Science and Technology, 42, 421-432, 10.1080/02786820802157823, 2008.

Swietlicki, E., Hansson, H. C., Hämeri, K., Svenningsson, B., Massling, A., McFiggans, G., McMurry, P. H., Petäjä, T., Tunved, P., Gysel, M., Topping, D., Weingartner, E., Baltensperger, U., Rissler, J., Wiedensohler, A., and Kulmala, M.: Hygroscopic properties of submicrometer atmospheric aerosol particles measured with H-TDMA instruments in various environments—a review, Tellus B: Chemical and Physical Meteorology, 60, 432-469, 10.1111/j.1600-0889.2008.00350.x, 2008.

Swietlicki, E., Hansson, H. C., Hämeri, K., Svenningsson, B., Massling, A., McFiggans, G., McMurry, P. H., Petäjä, T., Tunved, P., Gysel, M., Topping, D., Weingartner, E., Baltensperger, U., Rissler, J., Wiedensohler, A., and Kulmala, M.: Hygroscopic properties of submicrometer atmospheric aerosol particles measured with H-TDMA instruments in various environments—a review, Tellus B: Chemical and Physical Meteorology, 60, 432-469, 10.1111/j.1600-0889.2008.00350.x, 2017.

Tang, M., Chan, C. K., Li, Y. J., Su, H., Ma, Q., Wu, Z., Zhang, G., Wang, Z., Ge, M., Hu, M., He, H., and Wang, X.: A review of experimental techniques for aerosol hygroscopicity studies, Atmospheric Chemistry and Physics, 19, 12631-12686, 10.5194/acp-19-12631-2019, 2019.

Twomey, S.: Pollution and the planetary albedo, Atmospheric Environment (1967), 8, 1251-1256, http://dx.doi.org/10.1016/0004-6981(74)90004-3, 1974.

Voutilainen, A., Stratmann, F., and Kaipio, J. P.: A NON-HOMOGENEOUS REGULARIZATION METHOD FOR THE ESTIMATION OF NARROW AEROSOL SIZE DISTRIBUTIONS, J Aerosol Sci, 31, 1433-1445, https://doi.org/10.1016/S0021-8502(00)00044-6, 2000.

Wiedensohler, A., Lütkemeier, E., Feldpausch, M., and Helsper, C.: Investigation of the bipolar charge distribution at various gas conditions, J Aerosol Sci, 17, 413-416, https://doi.org/10.1016/0021-8502(86)90118-7, 1986.

Wu, Z., Wang, Y., Tan, T., Zhu, Y., Li, M., Shang, D., Wang, H., Lu, K., Guo, S., Zeng, L., and Zhang, Y.: Aerosol Liquid Water Driven by Anthropogenic Inorganic Salts: Implying Its Key Role in Haze Formation over the North China Plain, Environmental Science & Technology Letters, 5, 160-166, 10.1021/acs.estlett.8b00021, 2018.

Xu, W., Kuang, Y., Bian, Y., Liu, L., Li, F., Wang, Y., Xue, B., Luo, B., Huang, S., Yuan, B., Zhao, P., and Shao, M.: Current Challenges in Visibility Improvement in Southern China, Environmental Science & Technology Letters, 7, 395-401, 10.1021/acs.estlett.0c00274, 2020.

Zhao, G., Tao, J., Kuang, Y., Shen, C., Yu, Y., and Zhao, C.: Role of black carbon mass size distribution in the direct aerosol radiative forcing, Atmos. Chem. Phys., 19, 13175-13188, 10.5194/acp-19-13175-2019, 2019.